

5. Synthesis

5.1 Overview

The recent geomorphic evolution of the southern Firth is closely linked to historical increases in sediment loads following large-scale catchment deforestation and river-engineering works (1850s–1920s). An estimated 44 million m³ of mud was deposited in the southern Firth (south of Kaiāua) and lower Waihou River during a *c.* 40-year period up to 1918 (Ministry of Works files, 1919-1975, section 2.2 of present report). This deposit is equivalent to an estimated *c.* 300 years of the suspended sediment loads delivered by the Waihou and Piako Rivers to the Firth today. Distributed evenly over the 200 km² of seabed of the southern Firth the deposit would be *c.* 0.18 m thick. Hume and Dahm (1992) analysed sediment cores collected from the subtidal basin north of the Waihou River mouth between 1.5 and 6 m below chart datum. Pollen dating indicated that the top 0.05–0.2 m of these muddy sediments had been deposited since the mid-1800s. Naish (1990) has also calculated average SAR of ≤ 2 mm yr⁻¹ from radiocarbon dating for the muddy sediments deposited in the central Firth over the last several thousand years. Although there is potential for substantial uncertainty in sedimentation estimates based on comparison of historical hydrographic surveys (e.g., Harris, 1993), estimates for the southern Firth are consistent with the core data. Historical accounts of river and estuary sedimentation associated with deforestation and gold-mining activities in the Waihou catchment also indicate that large quantities of mud were discharged to the southern Firth (Brownell, 2004).

The sediment cores record the physical effects of this mud influx on the Firth. Below the base of the 0.8–1.6-m thick homogenous mud layer at *c.* +0.2-m MSL are the original laminated silts and sands that are characteristic of energetic mixed-sediment intertidal-flats (Reineck and Singh, 1980). The abrupt transition to a pure-mud substrate records this fundamental change in the sediments and geomorphology of the southern Firth. This process has initiated a sequence of large-scale environmental changes, which include the rapid mangrove-habitat expansion that began in the 1950s, and continues today. Similar environmental changes have occurred in other New Zealand estuaries. However, the rate and magnitude of these changes has been much larger in the Firth.

5.2 Mangrove-habitat expansion

The detailed chronology of mudflat sedimentation patterns and the historical aerial photographs enable the timing of major mangrove-seedling recruitment events and resulting forest-expansion to be refined:

- Event one: early-1950s
- Event two: mid-1960s
- Event three: mid-1980s
- Event four: early-1990s.

The aerial photographs show that the forest fringe has extended from LC-10 to LC-11 in the decade since 1996. This is primarily due to the growth of juvenile mangroves that were present on the mudflats in 1996 rather than seedling recruitment. By 2006 there was *c.* 741 hectares of mangrove forest between the Waitakaruru and Piako River mouths. Figure 5.1 summarises historical increases in mangrove habitat in the southern Firth since 1950.

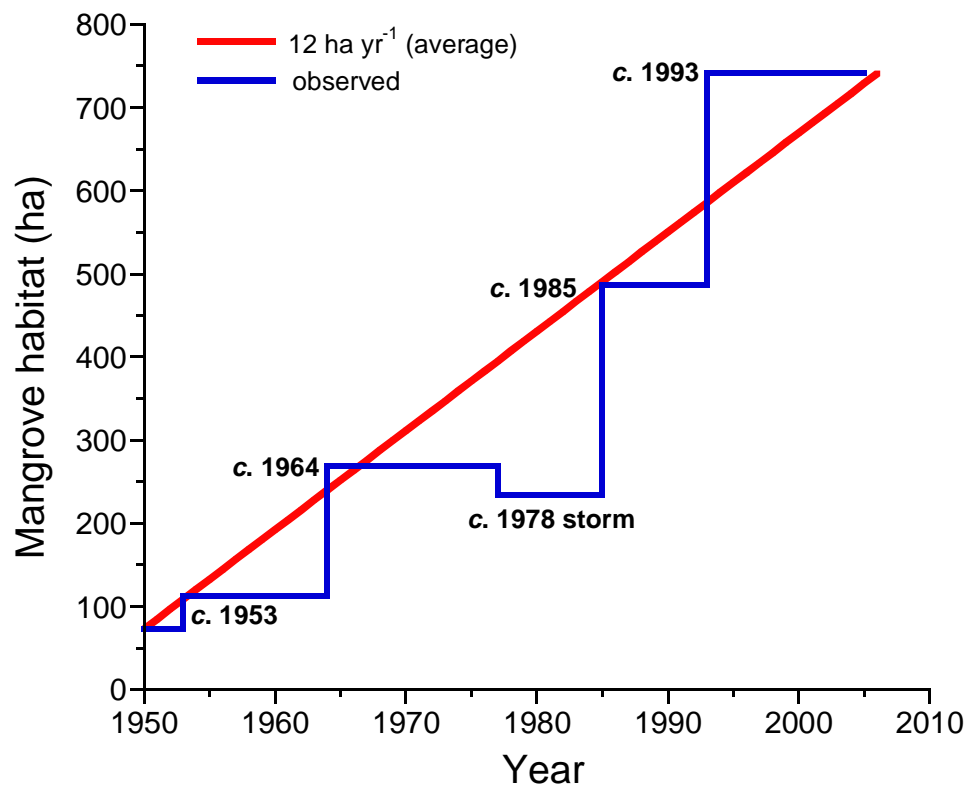


Figure 5.1 Mangrove-habitat expansion in the southern Firth since 1950. The rate of habitat expansion during this period has averaged $c. 12 \text{ ha yr}^{-1}$ (red line). The aerial photographs and sediment cores show that major seedling recruitment events and consequent habitat expansion has been infrequent and rare (blue line). The timing of these recruitment events is shown. Some 35 ha of fringing forest was lost during a storm in 1978. This value is probably a conservative estimate (section 5.4)

The historical reconstruction of mangrove-habitat expansion in the southern Firth shows that this process has occurred episodically and infrequently. The timing of these major recruitment events can be determined with confidence due to the comprehensive aerial-photographic record, complimentary radioisotope dating and the high temporal resolution of the dated sediment cores due to the rapid sedimentation.

Figure 5.2 shows the cross-shore variation in mangrove-tree canopy height and identifies the timing of the major forest expansion events.

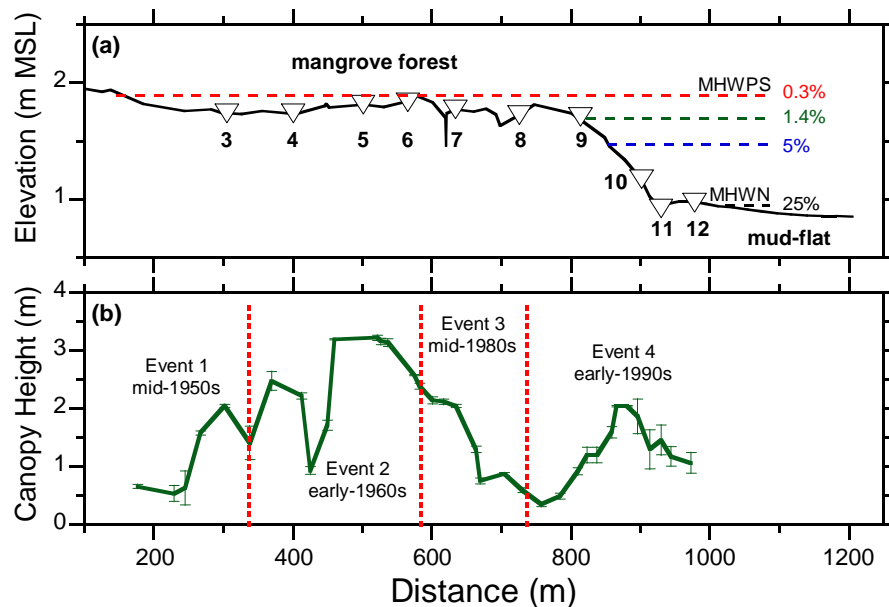


Figure 5.2 Transect B: (a) surface elevation, duration of tidal inundation (% of total time) and core locations (LC-3 to 12); (b) average canopy height (std. error = 0.01–0.03 m). The timings of major mangrove-seedling recruitment events are also shown (source: Swales et al. 2007).

The mangrove-forest that has developed on the mudflats since the mid-1950s displays a wide range of structure (Fig. 5.2b). Canopy height varies from $< 0.5\text{m}$ to 3.5m . Tree architecture also varies from open, spreading tree forms, which are indicative of trees that have grown in high-light environments without competition on colonizing edges, to trees with very straight trunks that have grown competing for available light.

A repeating pattern of taller trees giving way to short, dwarf trees was evident along the cross-shore transect. For example, the present forest fringe some 850 to 1000 m seaward of the 1952 shoreline gives way to a dwarf stand, with average canopy heights < 0.5 m. Landward of these dwarf mangroves, are found the tallest trees (450–600 m), with an average-canopy height of 3 m, where a well developed and older forest occurs.

The variation in canopy height observed for Event 2 suggests that this section of the old-growth forest represents two recruitment events rather than one. The sediment cores do not preserve any evidence of a second recruitment event, such as between-core differences in the timing of transitions from mudflat to mangrove fringe. Aerial photographs taken in 1963 and 1977 are also too infrequent to resolve this question. It is notable, however, that the canopy height variations along Transect B closely agree with the major phases of forest expansion that we have identified, so that the possibility that two recruitment events occurred during the 1963–1977 period cannot be discarded.

In many mangrove ecosystems canopy height reduces with distance from the seaward fringe. This reflects a reduction in tidal-water, nutrient and sediment inputs and an increase in salinity as evaporation exceeds tidal recharge (Smith, 1992). In the Firth, the complex variation in forest structure reflects the multiple forest building events. This system provides an important case study of how mangrove forests develop through time, and a baseline to investigate how the functions of mangrove ecosystems change as they undergo succession.

Swales et al. (2007) conclude that mortality of propagules and seedlings on the mudflat is primarily controlled by episodic wave-driven erosion of the substrate in which the seedlings are rooted. In southern Australia, wind and wave conditions are also the most important factors influencing *A. marina* seedling mortality in estuaries (Clarke and Myerscough 1991). The early development of seedlings on the mud flat indicates that conditions are suitable for growth in the absence of physical disturbance (Swales et al. 2007). The repeating pattern of tall seaward-fringing forest and short/dwarf forest landward and observed high seedling mortality on the mudflats suggests that major phases of mangrove-habitat expansion have occurred infrequently and likely coincide with extended periods of unusually calm weather conditions that are required for successful seedling establishment. This observation implies that a direct link exists between climate and mangrove-habitat expansion in the southern Firth of Thames. Further investigation of the interactions between physical processes and mangrove ecology are likely to yield new insights and provide information for management of mangrove habitat.

5.3 Sedimentation processes

5.3.1 Particle-size changes

Sediment cores LC-3 to LC-8 collected in the mangrove forest growing on the upper-intertidal mud platform sample sediments down to -0.1 m MSL elevation. Particle-size profiles show that sediments deposited in the mangrove forest are composed of homogenous muds, with median (D_{50}) and mean particle diameters of $\leq 20 \mu\text{m}$ (Figs. 5.3a–c). Wet sediment bulk sediment densities vary between 1 and 2.4 g cm^{-3} . Dry-sediment bulk densities (DBD) in these homogenous muds are uniformly low, with DBD values averaging 0.5 g cm^{-3} (range: $0.3\text{-}0.75 \text{ g cm}^{-3}$). The *c.* 80% porosity or water content by volume of these low-density muds is estimated assuming a quartz-feldspar mineral density of 2.6 g cm^{-3} .

Located near the seaward limit of the mud platform, core LC-8 shows an abrupt increase in particle size below 1.6-m depth (Fig. 5.3c). Basal sediments at 1.85-m depth are fine-sandy muds containing 10% fine sand $\leq 75 \mu\text{m}$. Cores LC-9 to LC-11 collected from the seaward-sloping mud beach on the forest fringe sample older sediments below *c.* 0.2 m MSL. These cores also show abrupt increases in particle size and sand content although at progressively shallower depths below the sediment surface (Fig. 5.3d–f). In core LC-9 the abrupt increase in particle size occurs at 1.5 m depth and at 0.7-m depth in LC-11, located at the base of the mud beach. The transition from homogenous-mud deposition to muddy-sands occurs at *c.* 0.2 m MSL. These muddy fine sands are composed of $\leq 70\%$ sand by volume and $\leq 165 \mu\text{m}$ diameter particles.

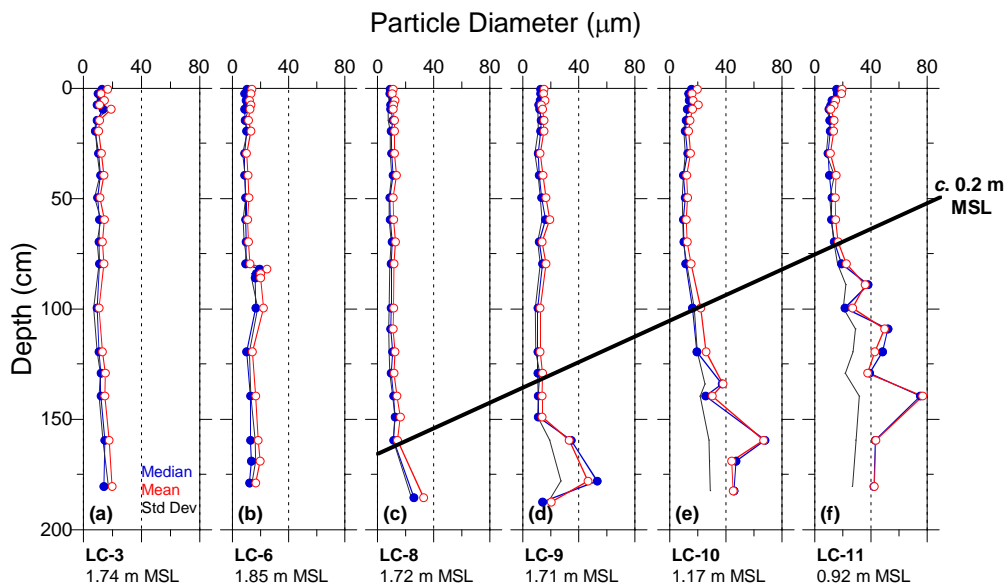


Figure 5.3: Particle-size profiles for selected cores from the mangrove-forest (LC-3 to -9), seaward fringe (LC-10) and adjacent mudflat (LC-11). Surface elevation at sites is also shown.

This shift from muddy-sand to pure-mud sedimentation indicates a fundamental change in the sedimentary regime of the southern Firth. ^{210}Pb dating shows that this transition from sand to mud occurred in the mid 1960s and, at most sites, years–decades before mangrove colonisation.

5.3.2 Sedimentation rates

The $^{210}\text{Pb}_{\text{us}}$ profiles preserved in the sediment cores display prominent changes in gradients that indicate changes in SAR over time and space (Fig. 5.4). The $^{210}\text{Pb}_{\text{us}}$ profiles are classified as two main types. Type one profiles (e.g., LC-3 to LC-5) exhibit a simple stair-step profile (Fig. 5.4a–c). These cores show a transition from muddy-sand and/or mudflat (**A**) to a mangrove-fringe environment (**B**) which is identified by an abrupt increase in SAR. Finally, SAR decline as old-growth forest develops and the forest fringe moves seawards (**C**). SAR decline as the old-growth forest is progressively isolated from the supply of sediment by elevation and distance from the mud flat.

Type two profiles differ from the simple stair-step sedimentation sequence. Some profiles, such as LC-6 and LC-10, display multiple stair-step forms and other profiles display progressive increases in SAR over time (Fig. 5.4e–f). An additional sedimentation phase, **A2-mudflat** was identified by comparing the dated profiles to the chronology of mangrove-habitat expansion. The A2 represents a period of accelerated mudflat sedimentation. These cores clearly show that the mudflat seaward of LC-6 began to accrete mud 2–10 times more rapidly and as much as twenty years before the arrival of mangroves (Fig. 5.4e–i).

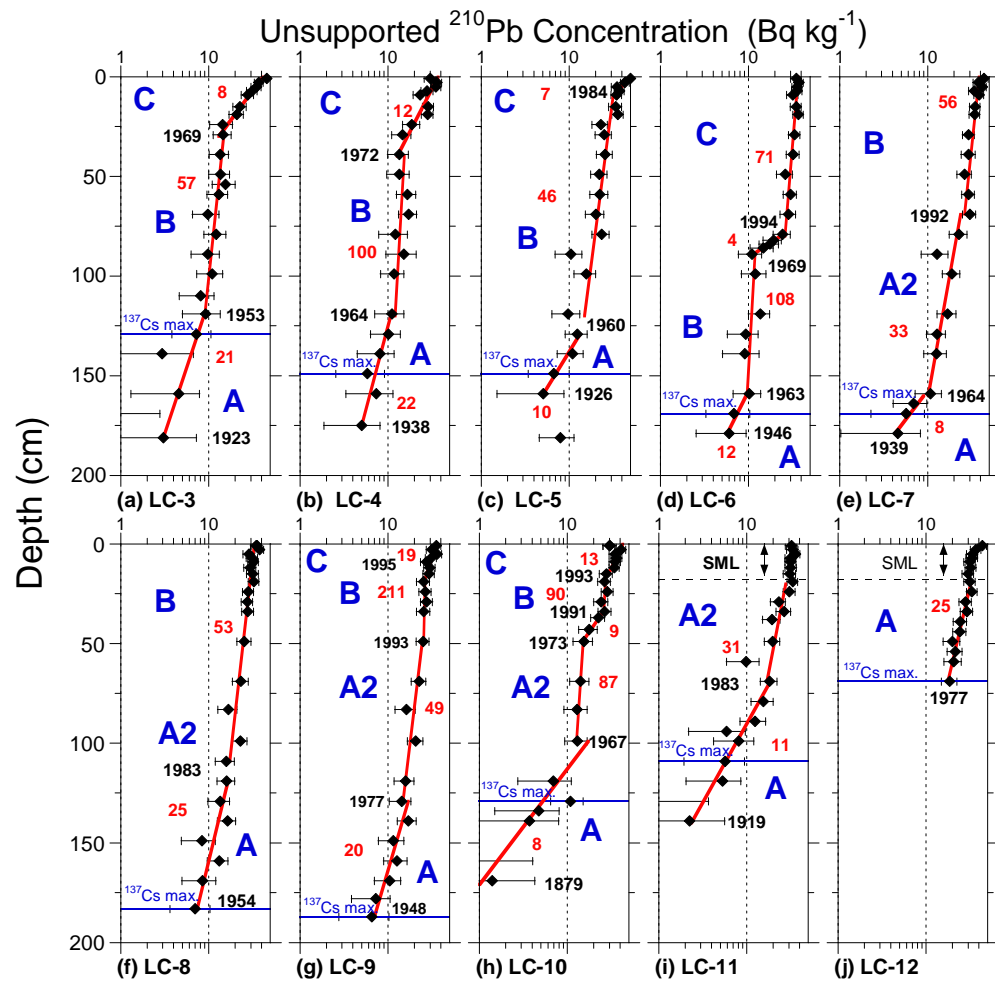


Figure 5.4: Cores LC-3 to LC-12 unsupported ²¹⁰Pb concentrations with 95% confidence intervals shown. Time-averaged sediment accumulation rate (red text) and maximum ¹³⁷Cs depth shown. The ages of the sediment deposit at inflection points in the ²¹⁰Pb profile. Also shown are the **sedimentation environments** (blue text): (A) muddy sand flat/mudflat; (A2) mudflat-2 – rapid sedimentation; (B) mangrove fringe; (C) mangrove forest.

Table 5.1 summarises the chronology of the changes in the sedimentary environment of the southern Firth that have occurred since the 1880s. This chronology has been reconstructed from the Transect B sediment cores and the historical aerial photographs.

Table 5.1: Chronology of changes in sedimentary environment of the tidal flat at Transect B based on ^{210}Pb dating, historical aerial photographs, x-radiographs and sediment properties. The surface elevation of the tidal flat (metres relative to mean sea level) at the end of each environmental period is shown in brackets.

| Core | Sedimentary Environment | | | | |
|-------|-------------------------|------------------|------------------|------------------|-----------|
| | Sandflat-A | Mudflat-A | Mudflat-A2 | Fringe-B | Forest-C |
| LC-3 | - | pre-1953 (0.55) | - | 1953–1969 (1.45) | post-1969 |
| LC-4 | - | pre-1964 (0.56) | - | 1964–1972 (1.36) | post-1972 |
| LC-5 | pre-1926 (0.2) | 1926–1960 (0.54) | - | 1960–1984 (1.64) | post-1984 |
| LC-6 | - | pre-1963 (0.24) | - | - | - |
| LC-7 | - | 1939–1964 (0.17) | 1964– 992 (1.0) | post-1992 (1.1) | - |
| LC-8 | pre-1965 (0.13) | 1965–1983 (0.58) | post-1983 | post-1983 | - |
| LC-9 | pre-1966 (0.21) | 1966–1977 (0.42) | 1977–1993 (1.21) | 1993–1995 (1.51) | post-1995 |
| LC-10 | pre-1967 (0.17) | - | 1967–1973 (0.67) | 1991-1993 (1.02) | post-1993 |
| LC-11 | pre-1983 (0.23) | - | 1983– | - | - |
| LC-12 | - | pre-2005 | - | - | - |

The LC-6 $^{210}\text{Pb}_{\text{us}}$ profile differs markedly from both profile types. In particular a marked horizontal offset or unconformity occurs in the $^{210}\text{Pb}_{\text{us}}$ concentration profile at 79–89-cm depth (Fig. 5.4d). The origin of this unconformity is discussed in section 5.5.

5.3.3 ^{210}Pb Budget and implications for fine-sediment fate

^{210}Pb is delivered to estuaries either directly (i.e., atmospheric deposition) or indirectly (i.e., attached to eroded soil particles). Most ^{210}Pb is delivered to the earth's surface with rainfall (Matthews, 1989) and ^{210}Pb delivered directly to estuaries is scavenged by fine mineral particles (clay and fine-silt) suspended in the water column. Once deposited, the $^{210}\text{Pb}_{\text{us}}$ decays at a constant rate over time (Appendix One).

Estuarine sediments will accumulate unsupported ^{210}Pb at a rate proportional to the mean annual ^{210}Pb atmospheric flux ($P_{\text{atmos.}}$), sedimentation rate and mud content. Radioisotopes, including ^{210}Pb and ^{137}Cs , are preferentially attached to clay particles because of their large numbers and surface area in comparison to larger silt and sand particles. The total amount or **inventory** of unsupported ^{210}Pb , $A(o)$, in a core can be used to estimate the mean annual ^{210}Pb supply rate (P) expressed as a flux, $\text{Bq cm}^{-2} \text{ yr}^{-1}$ (Appendix One). The $A(o)$ value is calculated for each core by integrating the unsupported ^{210}Pb concentration profiles. Down-core variations in unsupported ^{210}Pb reflect: (1) natural ^{210}Pb decay; (2) sediment bulk density; (3) mud content; and (4) depth and intensity of surface mixing.

The atmospheric ^{210}Pb flux ($P_{\text{atmos.}}$) has been measured by NIWA at monthly intervals since June 2002 at Howick (Auckland). Monthly ^{210}Pb fluxes show substantial variability (0.0001–0.002 $\text{Bq cm}^{-2} \text{ mo}^{-1}$). However annual fluxes (2003–2005) show much less variation, with $P_{\text{atmos.}} = 0.005 \text{ Bq cm}^{-2} \text{ yr}^{-1}$ ($s = \pm 1 \text{ Bq cm}^{-2} \text{ yr}^{-1}$). The $^{210}\text{Pb}_{\text{us}}$ inventories and measured ^{210}Pb atmospheric flux are used to infer the long-term fate of mud accumulating in the southern Firth of Thames.

Because ^{210}Pb labels mud, and in particular clay particles, the $^{210}\text{Pb}_{\text{us}}$ inventory and, in particular, P provides information about the long-term fate of mud in estuaries. For example, when $P > P_{\text{atmos.}}$ this indicates that mud is preferentially being deposited, a process referred to mud focusing or enrichment. By contrast $P < P_{\text{atmos.}}$ indicates that less mud is being deposited than would be expected and/or a large proportion of the mud is being winnowed from the site after initial deposition. Lastly, $P = P_{\text{atmos.}}$ when $^{210}\text{Pb}_{\text{us}}$ is accumulating in the sediment column in direct proportion to the atmospheric ^{210}Pb flux. The concentration factor (C) is given by the ratio $P/P_{\text{atmos.}}$ and indicates how P scales with the annual ^{210}Pb atmospheric flux.

Table 5.2 summarises $A(o)$, P and C values for the Transect B cores. The unsupported ^{210}Pb inventories (A) and mean annual supply rates (P) calculated for the long-cores display distinct spatial patterns. Inventories for cores LC-3 to LC-5 (1.27–1.59 Bq cm^{-2}) taken from the oldest mangrove forest that developed from the mid-1950s are similar. This reflects the similar depositional histories at these sites, with uniformly muddy sediment deposited at similar times and rates. Inventories in sediment cores LC-7 – LC-9 located in the forest established since the mid-1980s are also similar but larger than in the old forest. This mainly reflects the fact that the bulk of these muds have been more recently deposited and therefore have had less time for ^{210}Pb decay.

Table 5.2: Unsupported ^{210}Pb inventories, $A(o)$, mean annual supply rates (P) and concentration factors (C) for cores LC-3 to LC-11. Concentration factors are rounded up to the nearest integer.

| Core | $A(o)$ (Bq cm^{-2}) | P ($\text{Bq cm}^{-2} \text{ yr}^{-1}$) | C |
|-------|--------------------------------|---|-----|
| LC-3 | 1.27 | 0.039 | 8 |
| LC-4 | 1.40 | 0.044 | 9 |
| LC-5 | 1.59 | 0.050 | 10 |
| LC-6 | 3.75 | 0.117 | 23 |
| LC-7 | 1.87 | 0.058 | 12 |
| LC-8 | 1.73 | 0.054 | 11 |
| LC-9 | 1.75 | 0.055 | 11 |
| LC-10 | 1.21 | 0.038 | 8 |
| LC-11 | 0.15 | 0.005 | 1 |

At site LC-6, $A(o)$ is double that measured in any other core and reflects uniformly high unsupported ^{210}Pb concentrations ($30\text{--}40\text{ Bq kg}^{-1}$) in the top 0.8 m of the profile. This result implies ongoing rapid sedimentation at LC-6 (Fig. 5.4d) despite the fact that this site is now remote from the mudflat. Core LC-10, which is located in the present-day fringe, has a lower inventory than cores collected from the mature mangrove-forest. LC-11 located on the mudflat immediately seaward of the forest fringe has the lowest unsupported ^{210}Pb inventory.

Table 5.2 shows that sediments in the mangrove forest are accumulating 8–23 times more $^{210}\text{Pb}_{\text{us}}$ than would occur if supplied by direct atmospheric deposition alone (i.e., $C = 1$). On the mudflat at LC-11 $C = 1$. Swales et al. (2007) have shown from ^7Be and x-radiograph profiles that the mudflats are reworked to *c.* 7-cm depth over weeks–months. These laminated clays and silts are consistent with cycles of sediment resuspension by waves. The ^{210}Pb inventories and particle-size data for cores collected in the present study (Table 5.2, Fig. 5.3) indicate that the mangrove-forest has preferentially accumulated fine sediment.

5.3.4 Pollen Chronology

Pollen dating has been widely applied to reconstruct the long-term sedimentation chronology of and more recent human impacts of catchment deforestation on New Zealand estuaries (e.g., Hume and McGlone, 1986; Pocknall et al. 1989; Goff, 1997; Swales et al. 1997; Horrocks et al. 2000; Swales et al. 2002a, b; Ogden et al. 2006). Changes in the terrestrial vegetation assemblage are preserved in estuarine and lake sediments. Knowledge of the timing of these landcover changes are used to date sediment deposits (Appendix One). Sedimentation rates in the southern Firth have been ten-fold higher over the last 100 years than in Auckland and Coromandel estuaries. Consequently, the sediment cores only sample the period after catchment deforestation (mid-1800s – 1920s) so that we are unable to determine SAR based on the pollen profiles.

Pollen and spores sampled in the cores show a high degree of abrasion and fragmentation, which is a result of water transport. Pollen sources include atmospheric (i.e., wind and rain) and fluvial components. Pollen and spores associated with eroded soils are delivered to the Firth by rivers and distributed by tidal currents. The Waihou and Piako Rivers account for *c.* 95% of the catchment area and a large proportion of the sediment load delivered to the Firth. Thus, these rivers are most likely major contributors of pollen to the Firth. Native-forest pollens derived from the Hunua and

Coromandel Ranges are present in recent sediment deposits. The total fluvial or inwashed component includes an unknown proportion of reworked, older pollen. However, despite abrasion damage, the generally good preservation of pollens suggests that the reworked component is relatively small.

The presence of bracken spores indicates vegetation disturbance by repeated fires and reflects anthropogenic deforestation of the regional landscape. The presence of pine pollen throughout the cores indicates that these sediments have been deposited in European times. The dominance of the pollen sum by pine, rimu, bracken and *Cyathea* is not unexpected; because of their high production and widespread wind dispersal these pollen types tend to be well- or over-represented in pollen spectra. In this case this effect is exacerbated by fragmentation. An up-core increase over time of pine and grass pollen at the expense of bracken spores indicates expansion of pine plantations and a reduction in bracken due to pasture improvement.

The low abundance of mangrove pollen in the sediment cores is notable given that an extensive mangrove forest has developed in the southern Firth over the last 50 years. Modern and fossil pollen studies in New Zealand show that mangrove pollen is under-represented, with mangrove pollen not being recorded higher than 20% (Pocknall et al. 1989; Mildenhall 1994; Horrocks et al. 1998, 2000a, b, 2001; Ogden et al. 2006; Deng et al. 2006). Grey mangrove is insect-pollinated with low pollen production and highly localised pollen dispersal, so that mangrove pollen is always under-represented in estuarine sediments (Muller 1964). In the present study, mangrove pollen is rare even in modern surficial sediments so that mangrove shows extreme pollen under-representation.

Restricted dispersal of under-represented pollen types can provide detailed spatial information about mangrove-habitat expansion. For example, the presence of mangrove pollen above 80-cm depth in the sediment cores and not on the present-day forest fringe (LC-10) or adjacent mudflat (LC-11) is consistent with the known sequence of mangrove-habitat expansion. In the old forest, the ^{210}Pb age of mangrove pollen at 80-cm depth is consistent with mangrove arrival in the mid-1950s (LC-3) and mid 1960s (LC-4 to LC-6). A recent palynological study of Whangapoua Estuary (Great Barrier Island) showed that mangroves are highly discriminatory in relation to vegetation (Deng et al. 2006). The study also emphasised that pollen records of estuarine vegetation communities must be interpreted with caution as deposits can be subject to erosion and bioturbation.

5.4 Role of storms in mangrove-forest development

The role of infrequent catastrophic storms on mangrove-forest ecology has been documented in tropical mangrove systems. Most severe damage occurs to the largest mangrove trees. However, periodic destruction of mangrove forest in Caribbean systems appears to favour forest regeneration by promoting seedling recruitment in gaps resulting from tree loss (Roth, 1992). The influence of storms on long-term mangrove-forest development is relevant in the southern Firth because of the potential role of mangrove forest in mitigating the potential adverse effects of storms. These effects include shoreline erosion and inundation on low-lying coasts. In the present study, evidence of mudflat erosion and mangrove-forest damage by storms that occurred during the period 1977–1987 is provided by historical aerial-photographs and the sediment-core data.

Firstly, the aerial photographs show that core LC-6 occupied the seaward edge of the mangrove forest in 1977 and in 1987 this site was located on mudflat some 15-m seaward of the forest fringe (Fig. 5.5). This record clearly indicates substantial loss of mangrove trees on the forest fringe.

Comparison of the 1977 and 1987 photos for the entire southern Firth also show tree loss between Transects A and C (Fig. 5.6) on the forest fringe and in the old-growth forest landward of LC-6. This can be observed at Transect B (Fig. 5.3) and alongshore to Transect A (West) in the 1987 aerial photograph as areas of lighted-hued exposed mudflat. The total area affected by complete or partial mangrove-forest loss is estimated at *c.* 1.5 km². The abrupt change in forest type and a large tree trunk (10-m long and 40-cm diameter) stranded between LC5 and LC-6 is also evidence of forest disturbance at this time.

The degree of bed erosion required to dislodge a mature grey-mangrove tree can be estimated from the root habit and form of these plants. Grey mangroves are anchored to the top 0.5 m of the substrate by a network of shallow roots. Horizontal cable roots extend radially from the trunk, which are supported by downward-growing anchor roots (Janssen-Stelder et al. 2002). Thus, erosion of the mudflat to *c.* 0.5 m depth will be sufficient to detach even mature mangrove trees from the substrate.

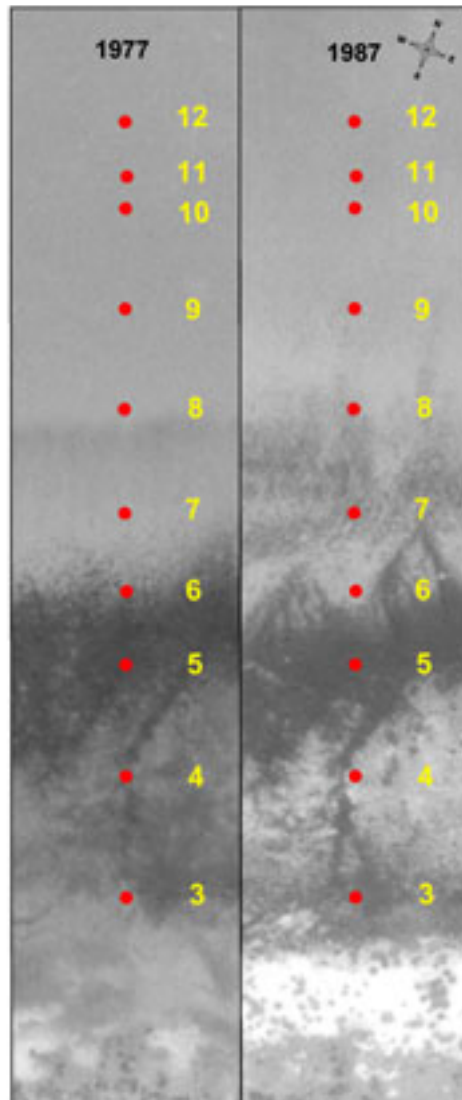


Figure 5.5: Mangrove-forest cover in 1977 and 1987 ± 100 m east and west of Transect B. The location of cores LC-3 to LC-12 are also shown.

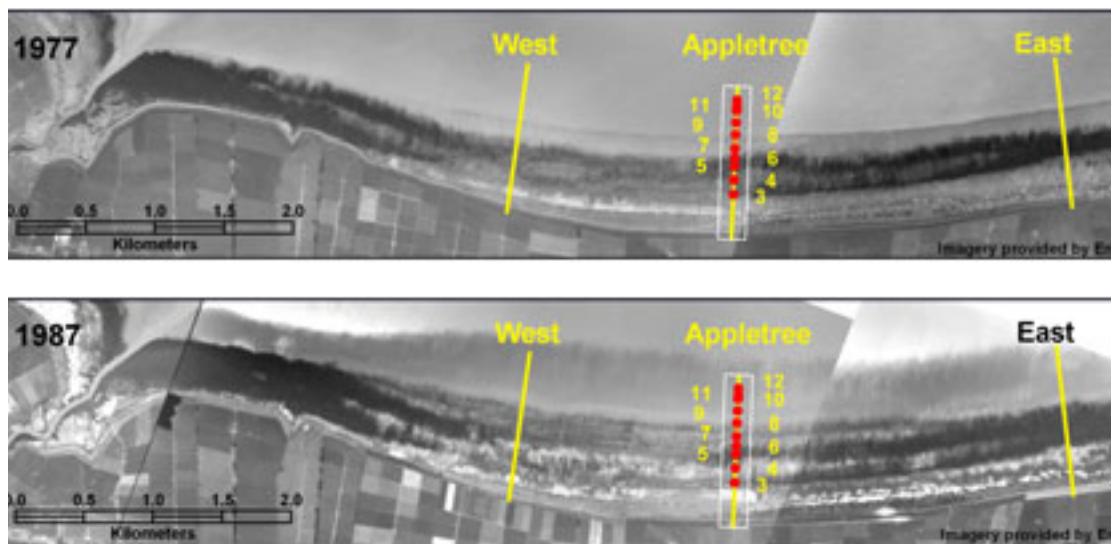


Figure 5.6: Mangrove-forest cover in 1977 and 1987, Waitakaruru River mouth to Transect C (East). The location of cores LC-3 to LC-12 along Transect B are also shown.

Figure 5.7 plots the radioisotope concentration and clay profiles for core LC-6. The $^{210}\text{Pb}_{\text{us}}$ profile differs markedly from LC-4 and LC-5, which also record the mangrove-seedling recruitment event that formed the old-growth forest in the 1950s – 1960s. Cores LC-4 and LC-5 display simple stair-step profiles that record the transition from mudflat to fringe to mature forest. By comparison, a marked horizontal offset or unconformity occurs in the LC-6 $^{210}\text{Pb}_{\text{us}}$ profile between 79–89-cm depth (Fig. 5.7a). An unconformity represents an interval of time during which sedimentation ceased or sediment erosion occurred, after which deposition of younger sediment resumed. The difference in age between the top and the bottom of the $^{210}\text{Pb}_{\text{us}}$ unconformity of *c.* 25 years was estimated based on the difference in $^{210}\text{Pb}_{\text{us}}$ concentrations of *c.* 11 Bq kg⁻¹. The apparent time-average SAR calculated across the unconformity is 4 mm yr⁻¹ (Fig. 5.7a). However, this apparent quarter-century age gap is not consistent with a SAR of 100 mm yr⁻¹ in the older underlying sediment deposit. This would indicate *c.* 2.5 m of vertical erosion of the mudflat, which is highly unlikely. Another factor that needs to be accounted for is the difference in the clay content of sediments across the unconformity. This is because clay content in particular, as well as sediment age, influences radioisotope concentrations in sediments.

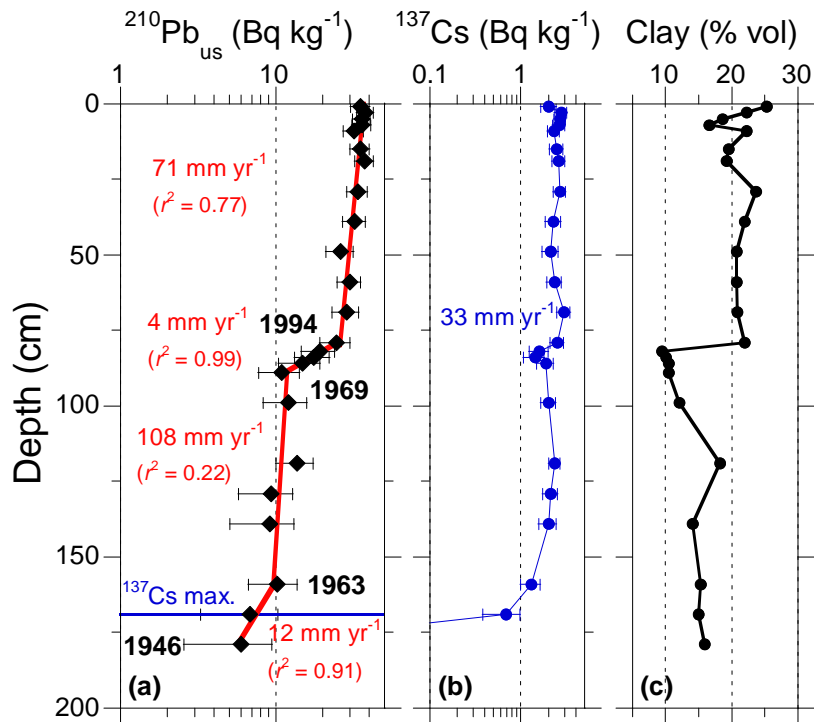


Figure 5.7: Core LC-6 sediment profiles: (a) unsupported ^{210}Pb concentrations with 95% confidence intervals shown. Time-averaged sediment accumulation rate (SAR) and co-efficient of determination (r^2) derived from fit to data (red line) and maximum ^{137}Cs depth. Also shown are the estimated ages of the sediment deposit at inflection points in the ^{210}Pb profile; (b) ^{137}Cs concentration profile with 95% confidence intervals shown and time averaged SAR; (c) Clay content of sediments expressed as a percentage of the total sample volume.

Figure 5.7c shows that the clay content of sediment below the $^{210}\text{Pb}_{\text{us}}$ unconformity is less than above the layer but does not vary within the unconformity. Consequently, the increase in $^{210}\text{Pb}_{\text{us}}$ concentration within the unconformity layer is due to deposition of younger sediments rather than particle-size effects. Near the top of the unconformity (79–82-cm depth), clay content increases markedly from 10% to 22% and distinguishes sediments deposited above the unconformity. Uniform clay content and intermediate $^{210}\text{Pb}_{\text{us}}$ concentrations within the unconformity are consistent with the erosion of older sediments, and subsequent mixing and deposition with younger sediments during a large-magnitude storm.

A more accurate estimate of the age difference between the top and bottom of the unconformity can be made by normalising the $^{210}\text{Pb}_{\text{us}}$ concentration for clay content. This yields an age difference of *c.* 4 years between the sediments immediately above and below the unconformity and indicate that *c.* 0.4 m of vertical erosion occurred during the storm event. Erosion of this layer would have exposed and detached the roots of even mature mangrove trees from the mudflat.

Review of storm events during the period 1977–1987 has identified the most likely candidate storm(s) that account for the observed storm effects in the southern Firth. Several storms impacted the north-east coast of the North Island during May–September 1978. The 19–20 July storm resulted in widespread and substantial beach and dune erosion along the east-coasts of the Northland and Coromandel Peninsulas. At Hahei, *c.* 1.3 m of sand eroded from the central part of the beach exposed a clay platform. This surface preserved wagon tracks and hoof prints, which was last exposed in the early 1900s (Hume, 1979). The 19–20 July 1978 storm was also the most potentially damaging storm in the Firth of Thames (section 2.6). This event produced strong north-east winds (Fig. 5.8) and a *c.* 0.6 m storm surge that coincided with perigean-spring high tides of +1.7 m MSL. Heavy wave action was reported at the mouth of the Waihou River (HCBRWB, 1978).

The July 1978 storm was the most damaging event to occur during the 1977–1987 period. Furthermore, the severity and scale of beach erosion that occurred during this storm along the North Island's north-east coast has not been exceeded since. The mudflat erosion indicated by core LC-6 and the mangrove-forest loss documented by the aerial photographs most likely result from the July 1978 storm. A similar magnitude storm that occurred in May 1938 also produced north-east gales and a storm surge that coincided with perigean-spring high tides (section 2.6). Storm waves breached the stopbank in several places between Waitakaruru and the Waihou River mouths and as a result some 350 km² of the lower Hauraki Plains was flooded by seawater.

The 1938 storm occurred before mangrove colonised the mudflat so that the coast was exposed to direct wave action at high tide. The mudflat elevation in 1938 was also 0.75–1.25 m lower than in 1978, so that waves were (1) likely less attenuated by bed friction and (2) wave-breaking would be delayed and occur closer to the shore.

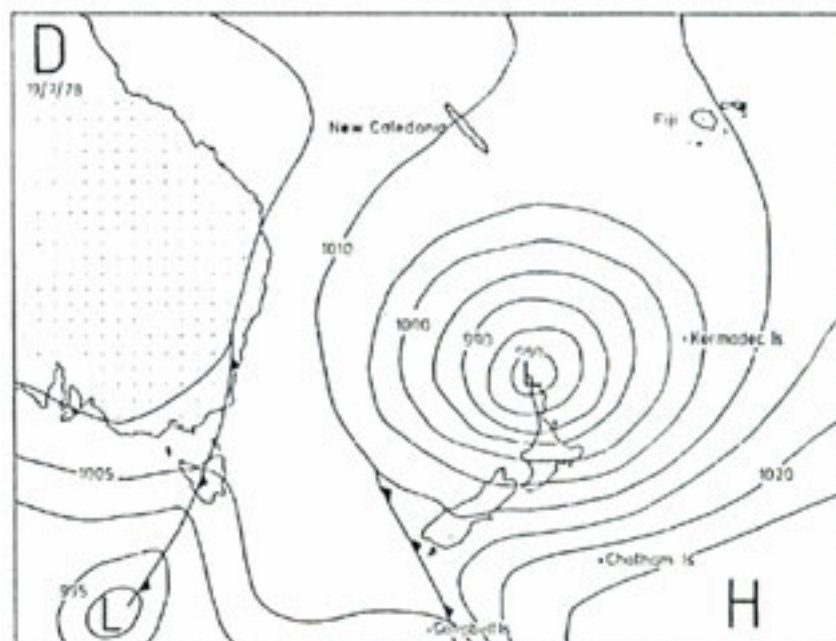


Figure 5.8: Synoptic weather chart of the south-west Pacific showing the situation at 1200 NZST, 19 July 1978. N.Z. Meteorological Service. (source: Hume, 1979).

5.5 Mangrove colonisation: triggers, controls and future habitat expansion

The lower-elevation limit (LEL) for grey-mangrove at mean sea level defines the maximum potential distribution of this mangrove species in North Island estuaries (section 1.1). Although mangrove propagules may establish below MSL, the physiological tolerances of grey mangroves preclude long-term survival and growth of seedlings below MSL (Clarke and Myerscough, 1993). Thus, the physical processes of sedimentation and tidal-flat formation ultimately determine mangrove colonisation and habitat expansion in estuaries.

Mangroves have existed on the elevated delta deposits at the outlets of the Waihou and Piako River for at least 200 years (section 1.1). The initial trigger for large-scale mangrove-habitat expansion was the large influx of mud from the mid-1800s onwards associated with catchment deforestation, mining and land conversion to pastoral agriculture. From the early 1900s onwards engineering works, associated with the construction of stopbanks and drainage channels, increasingly constrained flood runoff to river channels and is likely to have increased sediment delivery to the Firth. Much of this mud was deposited in the large subtidal compartment forming a layer up to several decimetres thick (Hume and Dahm, 1992).

Our sediment cores show that the lower intertidal flats were still composed of laminated muddy-sand flats up until the 1940s. These muddy-sand flats were rapidly buried under mud from the 1940s onwards, whereas mud had been depositing on the upper flats from the 1920s or earlier, where SAR averaged 20 mm yr^{-1} . Based on our understanding of fine-sediment dynamics in other North Island estuaries, mud deposited offshore in the shallow subtidal basin is likely to have been remobilised over time by waves (Green et al. 1997; Swales et al. 2004). The process of landward transport and accumulation of mud on tidal flats, due to settling- and scour-lag processes is well established (Postma, 1961). Mud deposits in the southern Firth are composed of fine silt and clay particles, with fall speeds $< 0.05 \text{ cm s}^{-1}$, that once suspended are readily transported. Transport velocities are also generally much lower than required for erosion so that these muds are progressively transported onshore and deposited.

Mangrove colonisation of these rapidly accreting mudflats did not occur until after surface elevations had built to $+0.55 \text{ m MSL}$. Mangrove first colonised the mudflat near LC-3 in the mid-1950s (section 4.1). Observations on the mudflat today indicate that mangrove-seedling recruitment is controlled by wind-waves (Swales et al. 2007). Thus initial mangrove colonisation would likely have coincided with an extended period of calm weather during summer–autumn when the mangrove seedlings were able to grow sufficiently large to withstand reworking of the mudflat by waves.

In nearby Tauranga Harbour, with its smaller wave fetch, the lower-elevation limit (LEL) for mangroves at wave-exposed sites is 0.3 m above MSL (Park, 2004). Tidal range is also likely to influence LEL because wave-energy expended at the bed partly depends on water depth due to water-column attenuation and bed-friction effects (Green et al. 1997; Swales et al. 2004). By normalising LEL for the southern Firth and Tauranga Harbour by the “king tide” amplitude we obtain a non-dimensional LEL of 0.3 for the southern Firth and Tauranga Harbour. This result suggests that the lowest elevation at which mangroves occur at wave-exposed sites is a fixed ratio of the tidal range. This type of approach could be used to develop a wave-exposure index to predict future mangrove-habitat expansion in estuaries.

In summary, the trigger for mangrove colonisation was the influx of mud to the Firth of Thames from the mid-1800s onwards due to large-scale catchment deforestation. Mangrove colonisation and habitat expansion on the mudflats since the mid-1950s has been primarily controlled by increases in surface elevation of the mudflat and wind climate. Presently, the seaward edge of the mangrove forest at $c. +0.9 \text{ m MSL}$ is 0.35 m above the LEL determined from core LC-3. At Transect B the mudflat slopes at 0.15° so that $c. 150 \text{ metres}$ of mudflat seaward of the mangrove-forest fringe is

potentially immediately available for future mangrove-habitat expansion. Mudflat surface elevation is increasing by 25 mm yr^{-1} , assuming zero sediment compaction, so that an additional *c.* 10 m yr^{-1} of mudflat is available for future mangrove-habitat expansion. This estimate is similar to the average rate of mangrove-habitat expansion of 12.5 m yr^{-1} observed in the southern Firth since the mid-1950s.

5.6 Large-scale morphological evolution

The geomorphic evolution of the tidal flats over the last 60 years was reconstructed based on: (1) the radioisotope geo-chronology; (2) core sediment data (i.e., x-radiographs, particle size, bulk density); (3) Transect-B intertidal-flat elevation profile; and (4) historical aerial photographs. Historical tidal-flat surfaces for years coinciding with aerial-photographs (1944–2002) were reconstructed as follows. The dated ^{210}Pb profiles at each core site were used to estimate the elevation of the tidal flat below the 2005 surface. We assumed that compaction of these recent mud deposits due to de-watering has been negligible, which is common in rapidly accumulating low-permeability mud. This assumption is supported by the uniform down-core dry-bulk sediment density profiles observed in the cores. The x-radiographs and particle-size data were used to identify spatial and temporal changes in sediment facies, as the tidal flat has evolved from a mixed mud-sand flat to a rapidly accreting mud flat colonised by mangroves in the mid-1950s.

Figure 5.9a shows how average sedimentation rates, based on ^{137}Cs dating, have varied across the mangrove forest over the last 50 years. SAR in the old-growth forest landward of LC-6 have averaged $< 30 \text{ mm yr}^{-1}$. The sediment depocentre, with maximum ^{137}Cs SAR $\geq 36 \text{ mm yr}^{-1}$, coincides with the mudflat seaward of LC-6, that was most recently colonised by mangroves. This cross-shore gradient in sedimentation reflects the geomorphic development of the mudflat and historical sequence of mangrove-habitat expansion. The morphological reconstruction that follows shows how the intertidal flat has evolved over the last sixty years (Fig. 5.9b). The sequence of mangrove-habitat expansion and tidal-flat morphology at Transect B is similar for the southern shore of the Firth so that this reconstruction is representative. The use of data from core LC-6 for the reconstruction is limited by the uncertainty in dating sediments within the $^{210}\text{Pb}_{\text{us}}$ profile unconformity at 79–89-cm depth (section 5.4). For sediments below the unconformity, we use the maximum ^{137}Cs depth to date sediments at 169-cm to 1953 AD as well as the ^{210}Pb SAR to estimate the elevation of the mudflat surface at LC-6 in 1944, 1952 and 1963. This results in a small difference in the ages (i.e., -2 years) of the inflection points in the $^{210}\text{Pb}_{\text{us}}$ profile (Fig. 5.4d).

Until the mid-1940s, the tidal flats were composed of gently-sloping muddy-sand flats between +0.4 and -0.5 m MSL. Tidal-flat sediments were laminated silts and fine sands characteristic of an energetic mixed-sediment intertidal-flat environment (Rhineck and Singh, 1980). The absence of sand at the base of cores LC-3 to LC-5 indicates that the upper flat was more muddy than further down the flat. Cores LC-10 and LC-11 provide clear sedimentological evidence of a shift from sand to mud from the 1940s onwards and by the mid-1960s the former muddy-sand flat had been replaced by mudflat. This environmental transition occurs at *c.* 0.2 m above MSL.

Mangrove began to colonise the upper mudflat at LC-3 in the mid-1950s and subsequently expanded seawards to LC-6 by the mid-1960s. Mud rapidly accumulated on the seaward fringe of this prograding mangrove forest. By the mid-1970s surface elevations in the old-growth forest at +1.4 – 1.5 m MSL were one metre above the adjacent mudflat, exceeded MHWN (+1 m MSL) and were close to MHWS tide level (+1.6 m MSL). Thus, by the mid-1970s the old-growth mangrove forest was infrequently supplied with suspended sediments transported by the tide. The old-growth forest was also being progressively isolated from the mudflat and the main sediment supply, with large quantities of sediment being trapped and deposited in the seaward fringe of the forest at LC-6 where SAR averaged 100 mm yr⁻¹. Thus, sedimentation rates within the old-growth forest substantially declined after the mid-1970s (Fig. 5.9b), with surface elevations increasing by ≤ 0.5 m over the last 30 years.

While mangrove colonised the upper-intertidal area in the mid-1960s, sedimentation rates increased 2–10 fold on the mudflat seaward of LC-6 (A2, Fig. 5.9b). Why SAR increased on the mudflat years before mangroves arrived is not clear. Possible explanations include: (1) an increase in mud delivery to the Firth; (2) increased remobilisation of mud deposits elsewhere in the Firth; and (3) changes in local hydrodynamic conditions due to mudflat accretion and/or elevated suspended-sediment concentrations (i.e., fluid muds) resulting in wave-height attenuation. For example, mud deposition on low-energy intertidal flats due to up-wind wave attenuation by bed-friction has been observed in the Manukau Harbour (Swales et al. 2004).

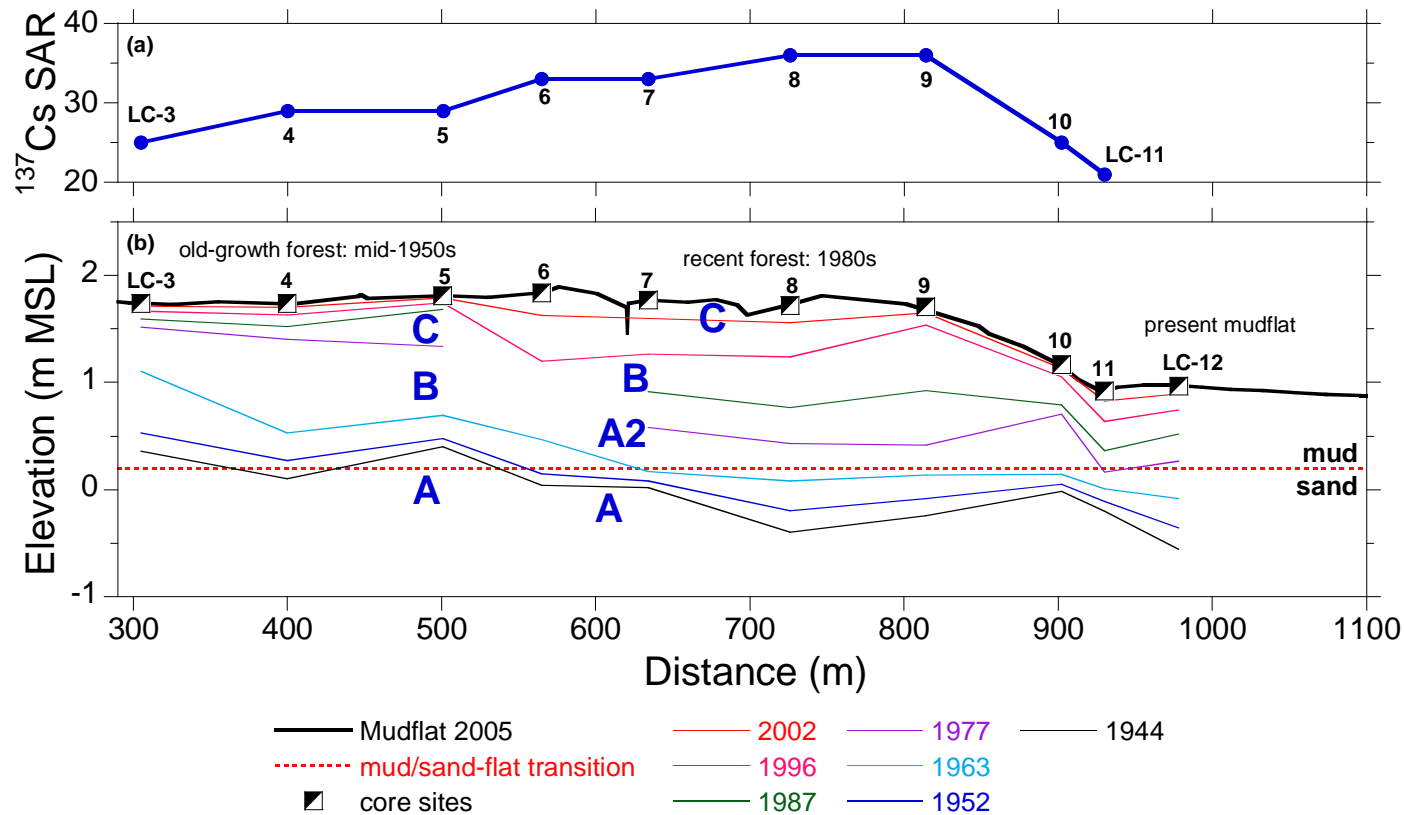


Figure 5.9: Transect B: (a) average sediment accumulation rates (SAR, mm yr⁻¹) based on maximum ^{137}Cs depth; (b) reconstruction of mudflat morphological development (1940s to present). Historical surface elevations have been calculated for years corresponding with aerial-photographs. **Sedimentation environments** are indicated by the blue text: (A) muddy sand flat/ mudflat; (A2) mudflat-2 – rapid sedimentation; (B) mangrove fringe; (C) mangrove forest.

By the mid-1980s, this rapid mudflat sedimentation had formed a several-hundred metre wide platform 0.8–0.9 m above MSL between LC-6 and LC-10 (Fig. 5.9b). Mangrove colonised this mudflat platform seaward to LC-8. The next major seedling recruitment occurred in the early 1990s and extended the mangrove forest to LC-10. A distinctive feature of the 1996 Transect-B aerial photograph is the area of mudflat landward of the forest fringe between sites LC-8 and LC-9, with a sparse coverage of juvenile mangrove trees (Fig. 4.3b). This mudflat area within the mangrove forest was not unique to Transect B and extended several kilometres alongshore to the east and west (Fig. 4.2). By 2002 mangrove trees had grown and/or colonised this area, although remnants of the mudflat were still apparent (Fig. 4.3b). This mudflat within the forest is today occupied by dwarf mangrove (Fig. 5.2). The cores show that mud accumulation on the forest fringe at the time was substantially more rapid (LC-9, 200 mm yr⁻¹) than in the dwarf-mangrove forest (50 mm yr⁻¹). This lateral sedimentation gradient produced a 200-m wide and 0.4-m-deep basin within the mangrove forest (Fig. 5.9b). Suspended sediments were delivered to the basin by tidal creeks. These tidal creeks have shrunk as surface elevations increased and the tidal-exchange volume declined. Remnants of these tidal creeks can still be seen in the dwarf-mangrove forest today. The basin has rapidly infilled with mud during the last decade to form the wide platform at +1.71 – 1.84 m MSL that extends across the entire mangrove forest today. This platform is substantially above MHWS tide elevation at +1.6 m MSL, so that most of the forest is infrequently flooded by extreme high spring-tides and/or storm tides.

The formation of the basin also explains why rapid sedimentation continued at sites LC-6 – LC-8 despite being isolated from the mudflat by the forest fringe. Sedimentation rates are likely to have substantially reduced in recent years from the average 50–70 mm yr⁻¹ indicated by the ²¹⁰Pb_{us} profiles (Figs. 5.4e–f). Surface elevations today are similar to the old-growth forest were SAR have averaged ≤ 12 mm yr⁻¹ since the mid-1970s.

The reconstruction of the mudflat morphological evolution (Fig. 5.9) can be summarised as age-surface elevation (ASE) curves for the old-growth (cores 3–5) and recent (cores 7–9) mangrove forests. The ASE curves (Fig. 5.10) were constructed by averaging surface elevations for both sets of cores in years coinciding with aerial photographic coverage.

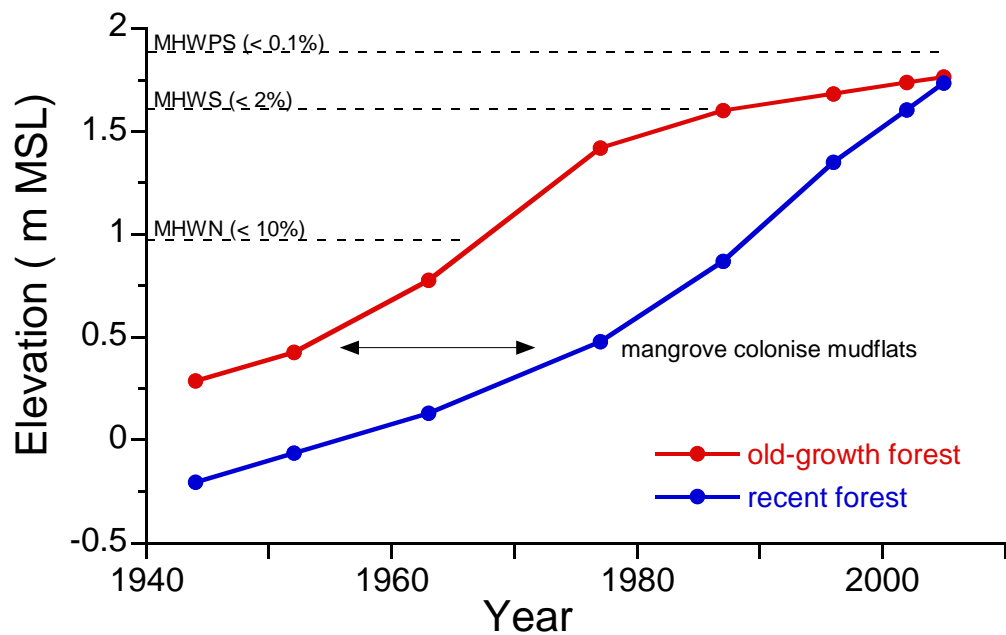


Figure 5.10: Age - surface elevation curves for the old-growth (cores 3–5, pre-1970s) and recent mangrove forests (cores 7–9, post-1970s). Also plotted are the mean high water neap, spring and perigean-spring tidal levels.

The ASE curves for the old-growth and recent mangrove forests display similarities and differences. Both ASE curves show an upward inflection at *c.* +0.5 m MSL as the mudflat is colonised by mangroves. This indicates an increase in the rate of surface elevation change although this occurs in several decades earlier, in the 1950s, for the old growth forest. By comparison, the elevation trajectories of the two forests have diverged markedly since the early 1980s. Rates of surface-elevation change in the old-growth forest decline from 65 mm yr⁻¹ (pre-1980s) to 9 mm yr⁻¹. This decline coincides with a progressive reduction in the duration of tidal inundation (Fig. 5.10). For example, by 1990 the average surface elevation in the old growth forest had reached MHWS level, with the forest at this elevation submerged <2% of the time. This pattern of initial rapid sedimentation followed by decline has also been observed in saltmarsh systems. Sedimentation proceeds rapidly following initial saltmarsh colonisation and then declines asymptotically as surfaces experience a progressive reduction in the frequency of tidal inundation (Allen, 1990; French, 1993). By comparison, surface elevations in the recent forest have continued to increase rapidly until the present time (Fig. 5.10). This trend is consistent with the infilling of the large sedimentation basin that developed in the recent forest immediately landward of the forest fringe and that has infilled with sediment since the mid-1990s. Today, average surface elevation in both forests is *c.* +1.74 m MSL, which is close to the extreme

upper limit of the tide. The future fate of the mangrove forests that have developed in the Firth of Thames during the last 50 years is considered in section 5.8.

5.7 Coastal-hazards mitigation by mangroves

Today mangrove forest has colonised c. 11 km² of intertidal mudflat in the southern Firth of Thames. The 7km² area of mangrove forest that has established between the Waitakaruru and Piako Rivers since the mid-1950s forms a continuous c. 700-m wide swath of vegetation. The mangroves have accelerated sedimentation forming a platform at +1.71 – 1.84 m MSL near the upper limit of the tidal range. In this section, the potential role of the mangrove forest in mitigating coastal erosion and inundation is evaluated.

5.7.1 Coastal erosion

The Hauraki Plains are protected from flooding by extreme storm tide by the earth stopbank that was constructed in the early 1900s. The stopbank has been subject to wave attack in the past. In May 1938, the stopbank was breached by storm waves at several locations between the Miranda and the Waihou River. Forty years later, the mangrove forest, that colonised the mudflat in the mid-1950s, protected the stopbank during a series of storms that occurred in 1978. Although mudflat erosion and widespread mangrove-forest loss occurred during the 1978 storms, the stopbank behind was protected from direct wave attack by the 300-m wide swath of mangrove forest (section 5.6). The mangrove forest has extended another 400-m seaward of the stopbank since the mid-1970s. Sea-bed surface elevations in the mangrove forest today average 0.7 m above the adjacent mudflat and provides an erosion buffer of c. 600 m³ per metre of shoreline. This is equivalent to 5.5 million m³ of sediment deposited between the Waitakaruru and Piako River mouths.

Mangrove forests have been reported to be more effective than concrete barriers or seawalls in dissipating wave and swell energy, reducing erosion, trapping sediments and stabilising shorelines. Wave-heights are rapidly attenuated by drag as waves propagate through the network of pneumatophores, trunks and canopy on the mangrove-forest fringe (e.g., Brinkman et al. 1997). Mangrove forests will have a substantially greater effect on attenuation of short waves (e.g., wind waves, swell and local/regional tsunami) than on long-wave phenomena such as storm surge and trans-Pacific tsunami, that have wave periods of 30 minutes or more. This arises because of the length of these waves, which carry behind them substantial volumes of water elevated above the predicted tide, which in the case of storm-tides can last a few hours around the high tide period. However the accompanying short waves or swell that ride

on the back of a storm tide would be effectively curtailed by the mangrove forest, resulting in a much less dynamic response in water level and run-up at the shoreline than usually occurs on the open coast from a storm tide.

The southern Firth of Thames is exposed to storm tides and waves generated by extra-tropical cyclones and extra-tropical depressions that develop in the mid-Tasman Sea. The potential for coastal erosion during large-magnitude storms is demonstrated by the historical and sediment-core records (sections 2.6 and 5.4). The existing mangrove-forest will continue to provide a high level of protection to the stopbank behind the forest from wave-induced coastal erosion.

5.7.2 Coastal Inundation

Inundation of the Hauraki Plains due to wave breaching and/or overtopping of the stopbank by storm tides or tsunami has the highest potential for large-scale and widespread damage to infrastructure, private property and direct impacts on the local economy. Road links to the Coromandel Peninsula and Bay of Plenty could also be affected.

Extreme tides

The distribution of high tides in a present-day climate context is shown by the bold black line in Figure 5.11, which is based on analysis of the Tararu tide-gauge record (from Bell and Goodhue, 2007).

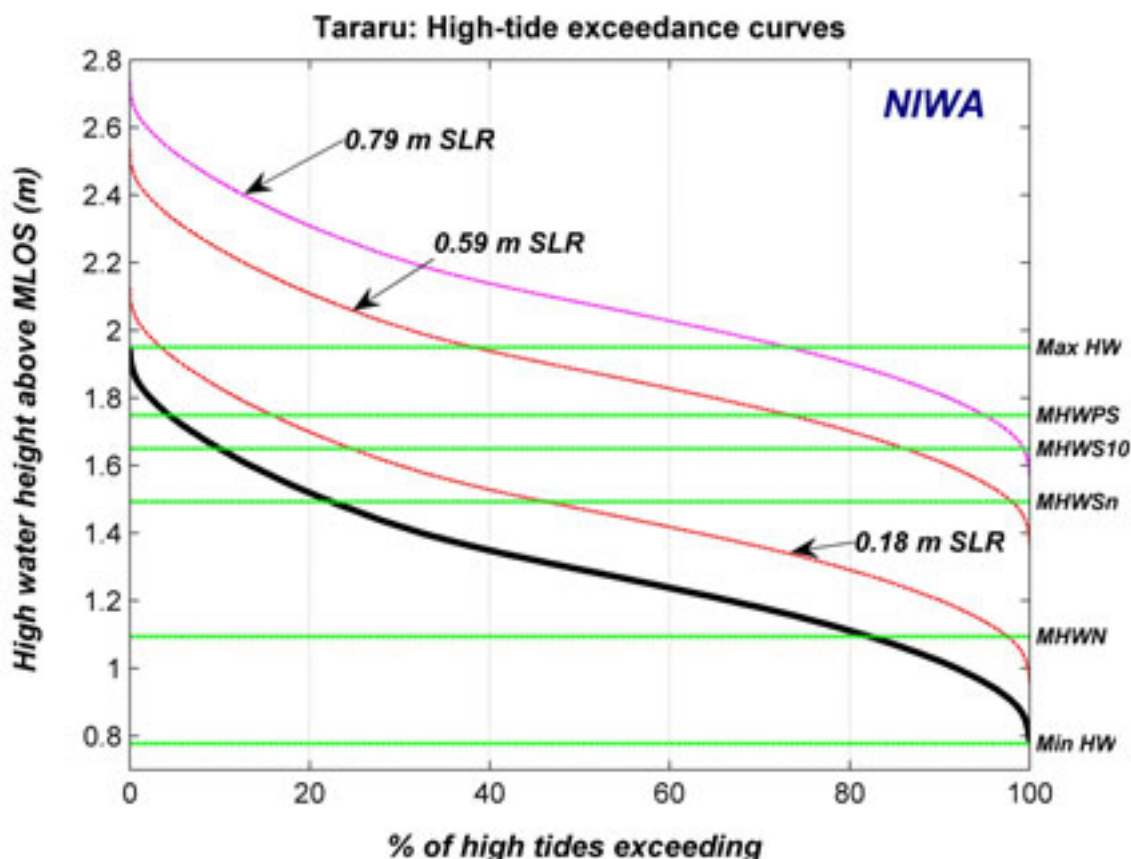


Figure 5.11: High-tide exceedance curve (thick line) based on 100-years of predicted high tides for 1990 to 2090 (excluding sea-level rise) from Bell & Goodhue (2007). The thinner lines show the high-tide exceedance distribution for three sea-level rise projections to 2090–99 from the IPCC 4th Assessment Report (IPCC, 2007). Annotations on the right-hand side for various tide marks relative to the present-day exceedance curve are listed below. [Heights relative to MLOS for present climate state, which is about 0.1 m above MVD–53].

Figure 5.11 key

- Max HW* = largest high water from 1990-2090 (excl. sea-level rise or SLR)
- MHWPS* = Mean High Water Perigean-Spring
- MHWS-10* = Mean High Water Spring exceeded by 10% of all high tides
- MHWsn* = Mean High Water Spring (using nautical definition: M_2+S_2 tidal constituents)
- MHWn* = Mean High Water Neap (nautical definition)
- Min HW* = smallest high water from 1990-2090 (excl. sea-level rise or SLR)

The exceedance level is relative to MLOS for the present climate state, which currently has mean-annual sea level at about +0.1 m MSL (i.e., MVD–53) datum.

Storm tides

Storm tides have historically exceeded +2.3 m MSL datum (section 4.2). The maximum recorded overtopping level in the Firth of Thames was +3 m MSL during

the 4–5 May 1938 storm. The predicted evening high tide on the 4 May 1938 was +1.74 m MSL (assuming MLOS was then at the same level as MVD-53), which categorises it as a perigean-spring tide (MHWPS). Because storm surge is unlikely to exceed one metre in New Zealand, the reported +3 m MSL storm tide is likely to have included wave set-up and/or run-up components (section 2.6). In the 1938 event, the stopbank was breached by storm waves at several locations between the Miranda and the Waihou River on 4 May. Some 350 km² of the Hauraki Plains were flooded by the sea, compounded by run-off from moderate-to-heavy rainfall (section 5. 4). At that time, the mangrove forest was restricted to delta deposits at the river mouths.

Tsunami

Tsunami from local, regional and remote sources have the potential to impact on the Firth of Thames. The relatively-short historical record shows that only remote-source tsunamis have generated wave run-up heights exceeding one metre (section 2.5).

Tsunami modelling of the local Kerepehi Fault (Chick et al. 2001) suggests a maximum vertical run-up height of 1–1.8 m. While the main direct impacts of such an event would occur on the east and west coasts of the Firth of Thames, the south coast could still be subject to rapid wave disturbances of around 5–15 minute periods including effects of tsunami wave resonance and wave reflection and possible bores up the rivers (section 2.5).

Remote tsunami sources exist all round the Pacific “Rim of Fire”, with South American sources posing the biggest threat for New Zealand. Recent modelling of remote South America tsunami sources for the Auckland region suggests that tsunami waves amplify somewhat as they propagate up the Firth, with the potential to reach a two-metre wave height with periods of 30 minutes up to 2 hours (E. Lane and J. Goff, NIWA pers comm.), although there would be some dissipation in water level through the mangrove forest. With these longer-period waves, the changes in water level will be more gradual than for local/regional sources, and hence unlikely to form a turbulent bore at the wave front. Although bores could still occur up river channels this is less likely for the longer-period tsunami.

It is well documented by ecologists and environmentalists in overseas literature that mangrove stands can substantially reduce the devastation caused by cyclones and tsunamis, a much underrated ecosystem service. Much of this work is based on observations in **tropical** mangrove forests, where areas that have escaped mangrove destruction, survived much better during cyclones or the 2004 Boxing Day tsunami. For example, a 1999 tropical cyclone ravaged Orissa in India claiming 10,000 lives.

The storm washed away several villages along the coast. However, villages in and around Bhitarkanika (India) were spared much of the cyclone's fury. This was attributed to the protection provided by the vast mangrove forest, which is the second largest mangrove forest in India. (For example web page:

<http://www.thehindubusinessline.com/2004/12/29/stories/2004122901121700.htm>).

The grey mangroves found in New Zealand have a shallow root system (i.e., ≤ 0.5 m of sediment column) and maybe more susceptible to detachment due to bed erosion than tropical mangrove species. Although we have no comparative data to test this idea, the extensive mangrove forest loss documented in the present study (Section 5.4), suggests that Manawa are vulnerable to wave erosion during large magnitude storms. The 1978 storm was a combination of a high-spring tide, 0.6-m storm surge and high, energetic waves, which eroded the mudflat with substantial mangrove-forest loss section 5.4. Today the mangrove forest has accumulated $600 \text{ m}^3 \text{ m}^{-1}$ of muddy sediment which provides a considerable erosion buffer besides the mangroves themselves, which also protect the shore from erosion by short-period waves.

Future sea-level rise

Since the mid 1800s, mean level of the sea around New Zealand has been rising. Over the last century the average linear relative rate has been 1.6 mm yr^{-1} (Hannah, 2004), or an absolute rise of 2.1 mm yr^{-1} if allowance for glacial-isostatic effects are included (although no other vertical tectonic movements are included). The Auckland record, which is the longest and highest quality of the datasets and is closest to the Firth, provides a relative sea-level rise rate of 1.3 mm yr^{-1} (Hannah, 2004). However, a recent update to 2005 (R. Bell, NIWA, pers. comm.) suggests that the long-term rate for Auckland is now 1.4 mm yr^{-1} due to higher mean sea levels over the last 5 years since the analysis was done by Hannah (2004). The average New Zealand rate over the last century is similar to the average global sea-level rise over the twentieth century of around $1.7\text{--}1.8 \text{ mm yr}^{-1}$.

Around New Zealand, without any definite data yet on present-day vertical land movements or differences in sea-level response in the South-Western Pacific compared to the global eustatic mean, it is currently assumed that sea-level change will be similar to the projections published by the Intergovernmental Panel on Climate Change (IPCC). To put this in context with both the long-term trend and the year-to-year fluctuations in mean level of the sea, Figure 5.12 shows the historic mean annual sea levels at Auckland over the last century and the latest IPCC (2007) projections to the decade 2090 to 2099.

The light blue band in Figure 5.12 shows the latest IPCC global mean sea level projections out to the decade 2090–2099. The range in increase in sea level, between 0.18 m to 0.59 m encompasses the full range of possible emission scenarios and computer model uncertainties. That is we do not know exactly how societies and economies will function in future and therefore how much greenhouse gases are going to be emitted over the coming century, which in turn will influence the rate of sea-level rise over this period and for millennia beyond 2100. Hence the sea-level estimates are based on different scenarios of greenhouse gas emissions over this time period (the range in sea level for a number of emission scenarios are shown by the vertical coloured lines (termed B1, A1T etc.) at the left hand side of the plot). The range in sea level projections encapsulated in each of the bands is due to the differences in projections for each emissions scenario provided by different global climate models.

The sea-level rise projections do include a contribution from land-ice flow from Greenland and Antarctica at the rates measured in the decade 1993 to 2003. But if this contribution increases, as expected, with average temperature increases in the future, then the upper ranges of the sea-level projections provided in the Fourth Assessment Report would increase by 0.1 to 0.2 m (dark blue band in Figure 5.12).

Therefore sea-level rise could potentially reach up to 0.8 m by the end of this century, but is more likely to be around 0.5 m, provided the melting of Greenland and Antarctica ice sheets doesn't accelerate. In the southern Firth, sedimentation rates on the bare mudflats have averaged *c.* 20 mm yr⁻¹ over the last 50 years. Mangrove colonisation and habitat expansion has accelerated sedimentation, with SAR averaging 50–100 mm yr⁻¹ on the forest fringe. Sedimentation rates in the old-growth forest have reduced to 7–12 mm yr⁻¹ due to the infrequency of tidal inundation (section 5.3.2). Thus, sedimentation rates over the last 50 years have exceeded predicted SLR rates over the next 100 years by as much as a factor of ten.

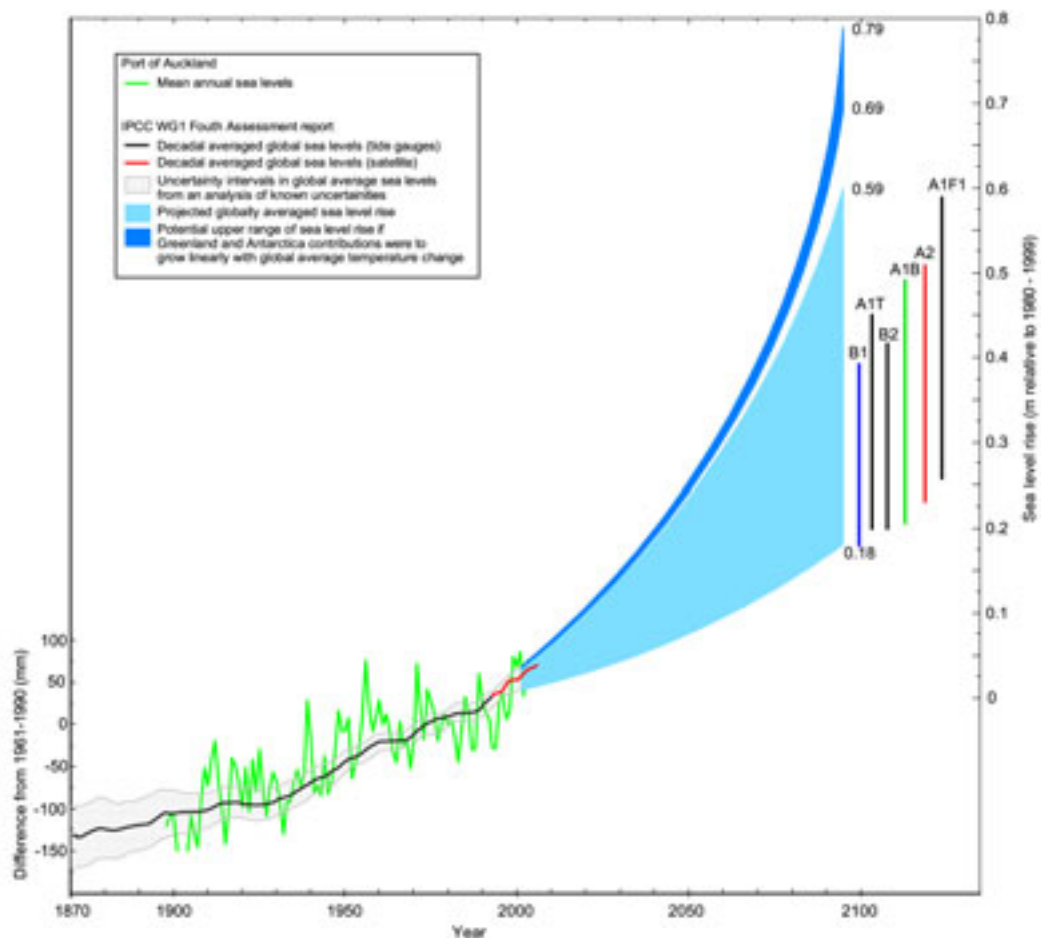


Figure 5.12: Past annual mean sea level change measure at the Port of Auckland up to 2005 and future global mean sea-level rise up to 2090–99 based on IPCC Fourth Assessment Report (IPCC, 2007) incorporating 6 different CO₂ emission scenarios (B1, A1T etc.) indicated by bars on right-hand side.

Overtopping potential and role of mangroves

The survey data from Transects A–C show that the farmland immediately behind the stopbank is 0.1 m below MSL and about two metres below the seabed elevation in the landward portion of the mangrove forest. The risk of inundation relates primarily to overtopping of the stopbank by extreme elevated sea levels, but in this analysis, failure of the stopbank through scour or seepage is not considered. In making a simplified assessment of the inundation hazard, based on just the three study transects, we assume a minimum stopbank crest level of *c.* +3.4 m MSL measured at Transect C (Figure 4.6). Possible scenarios for overtopping of the stopbank at any of these 3 transects and a brief assessment of the hazard are:

- **Extreme high tides:** the Mean HW Perigean-Spring tide mark (MHWPS) tide is presently at +1.85 m MSL datum (1.75 above MLOS) and the maximum HW tide does not presently exceed +2.05 m MSL datum (1.95 m above MLOS), as shown in Figure 4.5. This leaves about 1.3 m freeboard for the highest possible tide at the lowest point of the stopbank crest at any of the three transects. Therefore at this location, high tides alone will not cause inundation through overtopping. Because of the long length (period) of a tide wave, the mangrove forest will have a minor effect on retarding the level of the high tide at the stopbank;
- **Storm-tide:** overtopping from a storm surge coinciding with high spring or perigean tides is also unlikely at any of the three transects for the present-day climate and foreshore vegetation. Past recorded events have reached storm-tide levels of at least +2.3 m MSL. The swath of existing mangrove forest now provides an effective buffer to wave set-up and particularly run-up, so that stopbank overtopping by storm tides alone, at any of the three transects between the Piako and Waitakaruru River mouths, is unlikely to exceed the minimum stopbank height of around +3.4 m MSL in transect C for the present-day climate;
- **Tsunami:** the likelihood of inundation of the Hauraki Plains by a tsunami will depend on the height and period of the tsunami waves and the timing of the event with the astronomical tide (i.e., high or low, spring or neap). The level of protection from tsunami hazard provided by mangrove forests depends on the forest characteristics: bed elevation, width of forest, tree height and density. Certainly, the more slowly changing, but elevated water levels generated by long-period storm surges and those tsunamis generated remotely (e.g., South America) would still penetrate the forest causing elevated water levels at the backshore, but the dynamic waves/swell accompanying a storm or foaming fronts of shorter tsunami waves generated by local sources would be considerably attenuated by the swath of mangroves between the Piako and Waitakaruru River mouths, except where gaps occur. With the potential for up to a 2 m high tsunami wave height from a large magnitude, low-probability subduction-zone earthquake off South America, overtopping of the stopbank at transect C could occur if such an event coincided with a mean high water. Little work has been undertaken on the voracity of the grey mangrove species found in New Zealand to turbulent, erosive flows such as generated at the wave fronts of locally or regionally-generated tsunami. The results from this study indicate that such species of mangrove would have less effect on attenuating such short-period (e.g., 5 to 15 minute) tsunamis due to their shallower rooting systems

compared to tropical species. However the wide swath of mangrove forest that is now established still provides a formidable natural defence to the dynamic component of tsunamis;

- **Projected sea-level rise:** with projected sea levels of up to 0.8 m possible towards the end of this century, means that overtopping by storm-tide events (historically up to +2.3 m MSL) and would be possible, based on transect C. Climate change will not only cause a higher mean level of the sea, but is also likely to increase the intensity of storms (i.e., higher winds and lower central pressures), which in turn are likely to result in higher storm surges than is the case for the climate to date.

In summary, the mangrove forest, now firmly established between the Piako and Waitakaruru River mouths, provides a substantial ecosystem service by way of a substantial natural defence to tsunamis and wind waves and swell generated by storms. Parts of the forest, such as the seaward fringe, are likely to be damaged again in future by large persistent storms (that generate high waves) or future local/regional tsunamis, performing this ecosystem service but in so doing provides natural protection to the stopbank from the more dynamic aspects of coastal hazards. Eventually, sea-level rise and climate-change effects on storm intensity will render the current stopbank susceptible to storm-tide overtopping and elevate tsunami wave events that ride on the back of the prevailing sea level.

5.8 Future fate of the mangrove forest

The fate of mangrove-forests primarily depends on sediment-surface elevation increasing at a rate equal to or exceeding the rate of sea-level rise. This has previously been assessed by comparing sedimentation estimates from cores with rates of sea-level rise. However, this approach is too simplistic and ignores the potential effects of sediment compaction and biotic factors, such as root growth, which also influence surface elevation (Cahoon et al. 1999; McKee et al. 2007). Furthermore, the frequency and duration of flooding by tides and freshwater runoff varies with surface elevation and controls sediment delivery, substrate oxidation and plant growth.

Global warming primarily attributed to combustion of fossil fuels and release of greenhouse gases to the atmosphere is predicted to increase the rate of eustatic sea-level rise to an average of 5–8 mm yr⁻¹ by 2100 AD (IPCC, 2007). Mangrove and saltmarsh systems are sensitive to changes in sea level because of they depend on the maintenance of suitable upper-intertidal habitat. Mangroves and saltmarshes can respond to rising sea levels by either maintaining sediment-surface elevation and/or

retreating from the sea. McKee et al. (2007) reconstructed a Holocene (i.e., last 10,000 years) sea-level curve for Caribbean mangrove forests. These mangrove forests have accommodated eustatic SLR rates of up to 4 mm yr^{-1} primarily by peat deposition. In temperate environments, such as occur in New Zealand, mangrove forests have accumulated mainly inorganic mineral sediments. As sea level continues to rise, the maintenance of surface elevation will depend on continued sediment delivery to estuaries. In the southern Firth, SAR have substantially out-paced the historical rate of sea level rise, which has averaged 1.4 mm yr^{-1} since 1899 at the Port of Auckland. Consequently, the mangrove forest is now close to the upper limit of the tide so that the forest is very infrequently flooded. Today, sedimentation rates in the old-growth mangrove forest are likely to be much less than the average $7\text{--}12 \text{ mm yr}^{-1}$ over the last 30 years.

In many estuaries, including the Firth, shore-protection works and structures preclude the retreat of mangrove and saltmarsh communities from the rising sea. In the southern Firth, the mangrove forest can only respond to rising sea levels by maintaining surface elevation through sedimentation. This process is controlled by the feedback between surface elevation and the frequency and duration of tidal inundation. Over time, the surface elevation in the mangrove forest will continue to increase, with rising sea level, relative to the farmland protected by the stopbank. This sedimentation process has implications for the efficacy of the stopbanks and maintenance of drainage.

There is some uncertainty in how the mangrove forests will respond to climate change and rising sea levels in the future due to the complex feedbacks between the physical and biological processes controlling substrate elevation. For example, grey-mangrove in New Zealand is close to the southern latitudinal limit of mangrove globally. This limit primarily relates to air temperature and frost frequency and severity (Morrisey et al. 2007 review). Future climate warming is likely to influence mangrove growth and productivity, rainfall patterns, catchment runoff, sediment loads, wave activity and storm-tide frequency.

Sediment Elevation Tables (SET) have been widely used to monitor surface-elevation changes in mangrove forests and salt-marshes due to shallow subsidence and sedimentation (<http://www.pwrc.usgs.gov/set/>). This methodology has shown that SAR derived from cores is a poor predictor of **past** surface-elevation changes (Cahoon et al. 1999). The difficulties of predicting **future** surface-elevation changes based on historical SAR and therefore the fate of mangrove forests are more pronounced. To address this knowledge gap SET have been installed in the mangrove forest by NIWA and Environment Waikato. This monitoring programme will provide basic information for research and management of mangrove forests.

6. Summary

The grey mangrove (*Avicennia marina* subsp. *australasica*) or Manawa has rapidly colonised intertidal areas of the southern Firth of Thames during the last 50 years or so. Today, mangrove habitat occupies some 7 km² of former intertidal flat between the Piako and Waitakaruru Rivers and 11 km² in the southern Firth as a whole (section 1). The Firth is close to the southern limit of mangrove in New Zealand (*c.* 38°S), which occurs at Ohiwa Harbour (east coast) and Kawhia Harbour (west coast). Grey-mangrove seedlings can colonise intertidal areas down to about mean sea level (MSL) elevation, where they are submerged for < six hours per tide. Mangrove-habitat expansion has occurred in many North Island estuaries in recent decades as sediments delivered by rivers has built intertidal habitat suitable for mangrove colonisation. This process has accelerated over the last 150 years due to catchment deforestation and conversion to pastoral agriculture, with increased sediment loads delivered to estuaries.

The Firth of Thames is an 800 km² meso-tidal estuarine embayment and receives runoff from a 3600 km² land catchment. Currents, sea level and waves within the Firth are strongly linked to large-scale oceanographic and meteorological processes occurring within the wider Hauraki Gulf (section 2). The low-lying coast of the southern Firth is potentially exposed to erosion and inundation due to sea and swell waves, storm surge and tsunami.

The sequence of mangrove-habitat expansion in the southern Firth over the last 60 years was reconstructed from aerial photographs (1944, 1952, 1963, 1977, 1987, 1996, 2002 and 2006, section 3.1). Shore-normal elevation profiles were measured along three transects (A–C, January 2005) through the mangrove forest to: provide information on large-scale coastal morphology; relate bed elevations and sediment cores to MSL (*i.e.*, Moturiki Vertical Datum-1953; and provide information for the coastal erosion and inundation hazards assessment (section 3.2). Transects A–C were located at *c.* 2-km intervals alongshore and extended up to 1200-m seaward of the flood-defence stopbank landward of the mangrove forest (Fig. 1.1). Elevations were measured to ± 0.5 cm using a Geodimeter Model 464 total station.

Replicate sediment cores up to 1.9-m long were collected from the mangrove forest (sites LC-3 to LC-11) and adjacent mudflat (site LC-12) along Transect B, using a Livingston piston corer (section 3.3). SAR were estimated from the caesium-137 (¹³⁷Cs, *t*_{1/2} 30 yr) and unsupported lead-210 (²¹⁰Pb_{us}, half-life, *t*_{1/2}, 22.3 yr) concentration profiles. X-radiographs of the cores provide information on the fine-scale sedimentary fabric of sediments. Particle-size distribution (PSD) was determined

using a Galai CIS-100 stream-scanning laser particle sizer. The tide record at Tararu (37.133°S, 175.542°E) was analysed (section 3.4) to determine: the duration of tidal inundation of the present-day mangrove forest (2004–2006); and exceedance probability (%) for predicted high-tide levels (1900–1999 AD). The inundation time for specified vertical levels was determined for predicted tides, using tidal constituents for 2004–2006, and measured storm tides.

Aerial photographs show that mangrove stands were restricted to delta deposits at river mouths in the mid-1940s. We distinguish between **old-growth mangrove forest** that colonised the mudflats before the mid-1970s and **recent mangrove forest** that has established since that time. The distinction between old and recent mangrove forest is based on major differences in forest development and sedimentation histories (sections 4 and 5). The boundary between these forests occurs near site LC-6, which was located on the seaward fringe of the forest in 1977. The mangrove forest that has developed over the last 50 years is the result of only 4–5 major seedling-recruitment events that occurred in the early-1950s, mid-1960s, mid-1980s and early-1990s (Fig. 5.1). No major seedling recruitment has occurred in the last decade. Seedling mortality is primarily controlled by episodic wave-driven erosion of the mudflat surface. Seedling recruitment events are likely to coincide with extended periods of unusually calm weather conditions (Swales et al. 2007). This observation indicates a direct link exists between climate and mangrove-habitat expansion in the southern Firth of Thames.

The mangrove forest today at *c.* +1.7 m MSL is near the upper limit of the tide and is inundated < 3% of the time. The mean high water perigean spring (MHWPS) and MHSW tide levels are at +1.87 m MSL and +1.6 m MSL respectively. The highest measured storm-tide reached +2.33 m MSL on 18 September 2005, which included a 0.5-m storm surge. Storm tides increase the length of tidal inundation of the mangrove forest by *c.* 40% (i.e., 30 hrs/yr).

The recent geomorphic evolution of the southern Firth is closely linked to historical increases in sediment loads following catchment deforestation and river-engineering works (1850s–1920s). An estimated 44 million m³ of mud was deposited in the southern Firth (south of Kaiāua) and lower Waihou River during a *c.* 40-year period up to 1918. Distributed evenly over the 200 km² of seabed the deposit would be *c.* 0.18 m thick. Sediment cores collected along Transect B record the physical effects of this mud influx. Below the base of the 0.8–1.6-m thick mud layer at *c.* +0.2-m MSL are the original laminated silts and sands that are characteristic of energetic mixed-sediment intertidal-flats. The abrupt transition to a mud substrate which began in the 1920s records this fundamental change in the sediments and geomorphology of the

southern Firth. This process has initiated a sequence of large-scale environmental changes, which include the rapid mangrove-habitat expansion that began in the 1950s. Similar environmental changes have occurred in other New Zealand estuaries. However, the rate and magnitude of these changes has been much larger in the Firth.

The $^{210}\text{Pb}_{\text{us}}$ profiles show that sedimentation increased as mangroves colonised the mudflat then subsequently declined as the old-growth forest was progressively isolated from the mudflat by elevation and distance. Mudflat SAR averaged *c.* 20 mm yr⁻¹ before mangroves arrived in the mid-1950s and is similar to rates on the mudflat today. The cores also show that for a time the mudflat seaward of the old-growth forest accumulated sediment 2–10 times more rapidly (30–90 mm yr⁻¹) and as much as 20 years before mangroves arrived in the mid-1980s. The seaward advance of the mangrove forest is preserved in the cores by the abrupt increase in SAR (50–200 mm yr⁻¹) that occurred on the forest fringe. ^{210}Pb inventories and particle-size data indicate that the mangrove-forest has preferentially accumulated fine sediment (section 5.3). The cores sample sediments deposited after catchment deforestation so that we are unable to determine SAR based on the pollen profiles.

Reconstruction of tidal-flat evolution over the last 60 years (section 5.6) shows that rapid sedimentation in the old-growth mangrove forest had, by the mid-1970s, increased surface elevations one metre above the adjacent mudflat. This process markedly reduced tidal inundation and isolated the old-growth forest from the mudflat sediment supply, with surface elevations increasing by ≤ 0.5 m (7–12 mm yr⁻¹) over the last 30 years. Forest development following the most recent seedling recruitment event in the early 1990s has been complex. Seedlings adjacent to the mudflat grew rapidly. Between this emerging tall-tree fringe and the old-growth forest was an extensive mudflat with sparse coverage of small juvenile trees, which extended several kilometres alongshore (Fig. 4.2). For a short time, mud accumulation on the forest fringe (200 mm yr⁻¹) was substantially more rapid than in the dwarf-mangrove forest (50 mm yr⁻¹). This horizontal sedimentation gradient produced a 200-m wide and 0.4-m-deep basin within the mangrove forest (Fig. 5.9). By 2002, the size and density of trees on this mudflat had increased, which today is occupied by dwarf mangroves (section 5.2). Remnants of the tidal creeks that delivered mud to the basin remain in the dwarf-mangrove forest today. The basin has rapidly infilled during the last decade to form the wide platform at *c.* +1.75 m MSL that extends across the entire forest today.

The reconstruction of the tidal-flat evolution can be summarised as age-surface elevation (ASE) curves for the old-growth and recent mangrove forests. The ASE curves (Fig. 5.10) were constructed by averaging surface elevations for both sets of

cores in years coinciding with aerial photographic coverage. The ASE curves show an upward inflection at *c.* +0.5 m MSL as the mudflat is colonised by mangroves. This indicates an increase in the rate of surface elevation change although this occurs in several decades earlier (i.e., 1950s) for the old growth forest. The elevation trajectories of the two forests have diverged markedly since the early 1980s. In the old-growth forest, average rates of surface-elevation change decline from 65 mm yr⁻¹ (pre-1980s) to 9 mm yr⁻¹. This decline coincides with a progressive reduction in the duration of tidal inundation (Fig. 5.10). This pattern of initial rapid sedimentation followed by decline due to reduced frequency of tidal inundation has also been observed in saltmarsh systems (Allen, 1990; French, 1993). In the recent forest, surface elevations continued to increase rapidly until the present (Fig. 5.10), which is consistent with the infilling of the large basin that developed landward of the forest fringe in the mid-1990s. Today, average surface elevation in both forests are similar (+1.74 m MSL) and close to the extreme upper limit of the tide.

The aerial-photographs and sediment cores also preserve evidence of mudflat erosion and mangrove-forest damage by storms. At Transect B the forest fringe retreated *c.* 15 m between 1977 and 1987. Loss of an estimated 35 hectares of mangrove forest occurred along the seaward fringe and extensive damage to *c.* 1.5 km² of forest. Erosion of the mudflat to *c.* 0.5 m depth is sufficient to detach mature grey-mangrove trees from the substrate. An unconformity in the LC-6 ²¹⁰Pb_{us} concentration profile at 79–89-cm depth represents an interval of time during which sedimentation either ceased or sediment erosion occurred, after which sedimentation resumed. The unconformity represents an age difference of *c.* 4 years and is equivalent to *c.* 0.4 m of vertical erosion, which was sufficient to expose and detached the roots of mature mangrove trees from the mudflat. The most likely candidate storm is that which occurred in July 1978, which generated a 0.6-m storm surge and waves in the Firth that coincided with perigean-spring high tides. This storm also caused severe and widespread beach erosion along the North Island's north-east coast. The May 1938 storm was of a similar magnitude but without the protection provided by mangrove forest, storm waves breached the stopbank in several places and the sea flooded *c.* 350 km² of the lower Hauraki Plains.

Presently, the seaward edge of the mangrove forest at *c.* +0.9 m MSL is 0.35 m above the lower-elevation limit for seedling recruitment on the wave-exposed mudflat (section 5.5). The mudflat slopes at 0.15° so that *c.* 150 metres of mudflat seaward of the mangrove-forest fringe is potentially immediately available for future mangrove-habitat expansion. Mudflat surface elevation is increasing at 25 mm yr⁻¹ so that the area suitable for mangrove seedlings increases by *c.* 10 m yr⁻¹. This estimate is similar to the average rate of mangrove-habitat expansion of 12.5 m yr⁻¹ over the last 50 years.

The mangrove forest provides a number of ecosystem services, which mitigate the potential coastal erosion and inundation hazards that exist for the low-lying Hauraki Plains. Farmland immediately behind the stopbank is *c.* 0.1 m below MSL and *c.* 2 m below the seabed elevation in the mangrove forest. Sediment accumulated in the forest above the elevation of adjacent mudflat provides an erosion buffer of *c.* 600 m³ per metre of shoreline. The potential for coastal erosion during large-magnitude storms is demonstrated by historical events (sections 2.6 and 5.4). The present-day mangrove-forest will continue to provide a high level of protection to the stopbank behind the forest from wave-induced coastal erosion.

The risk of inundation relates primarily to overtopping of the stopbank by extreme elevated sea levels and future sea-level rise (SLR) due to global warming. In making this assessment of the inundation hazard, we assume a minimum stopbank crest level of *c.* +3.4 m MSL (Transect C) and that the mangrove forest is preserved. Inundation due to overtopping of the stopbank by storm tides or tsunami has the highest potential for large-scale and widespread damage to infrastructure and private property and direct impacts on the local economy. Although the mangrove forest will have a minimal effect on retarding the level of the high tide at the stopbank, extreme high tides will not cause inundation. Storm surge coinciding with high spring or perigean tides is also unlikely to cause overtopping at Transects A–C. The likelihood of inundation by tsunami will depend on the height and period of the tsunami waves and the timing of the event with the astronomical tide (section 5.7.2). The relatively-short historical record shows that only remote-source tsunamis have generated wave run-up heights exceeding one metre (section 2.5). The mangrove forest would likely have minimal effect on attenuating locally-generated short-period (e.g., 5 to 15 minute) tsunamis due to their shallow root systems but still provides a buffer to the dynamic component of tsunamis.

Since the mid 1800s, mean level of the sea around New Zealand has been rising. The long-term rate of relative sea level rise at Auckland (1899–2000) of 1.3 mm yr⁻¹ has increased to 1.4 mm yr⁻¹ (2001–2005). IPCC (2007) projections for SLR over the next 100 years range from 1.8 to 8 mm yr⁻¹. These predictions encompass the full range of greenhouse-gas emission scenarios and model uncertainties. In the southern Firth, sedimentation rates on the bare mudflats have averaged *c.* 20 mm yr⁻¹ over the last 50 years. Mangrove colonisation and habitat expansion has accelerated sedimentation, with SAR averaging 50–100 mm yr⁻¹ on the forest fringe. Sedimentation rates in the old-growth forest have reduced to 7–12 mm yr⁻¹ due to the infrequency of tidal inundation. Thus, sedimentation rates over the last 50 years have exceeded SLR predicted for the next 100 years by as much as a factor of ten. By comparison, SAR in Auckland, Waikato and Coromandel estuaries have averaged 2–4 mm yr⁻¹ over the last 50 years.

The fate of mangrove-forests primarily depends on sediment-surface elevation increasing at a rate equal to or exceeding SLR. This has previously been assessed by comparing sedimentation estimates from cores with rates of sea-level rise. However, this approach does not take into account the potential effects of sediment compaction and biotic factors, such as root growth, which also influence surface elevation. Mangrove systems are sensitive to changes in sea level because they depend on the maintenance of suitable intertidal habitat. Mangroves can respond to rising sea levels by either maintaining sediment-surface elevation and/or retreating from the sea. In many estuaries, shore-protection structures preclude the retreat of mangrove forest from the rising sea. In the southern Firth, the mangrove forest can only respond to rising sea levels by maintaining surface elevation through sedimentation. This sedimentation process has implications for the efficacy of the stopbanks and maintenance of drainage.

There is some uncertainty in how the mangrove forests will respond to climate change and rising sea levels in the future due to the complex feedbacks between the physical and biological processes controlling substrate elevation. Future climate warming is likely to influence mangrove growth and productivity, rainfall patterns, catchment runoff, sediment loads, wave activity and storm-tide frequency. Sediment Elevation Tables (SET) have been widely used to monitor surface-elevation changes in mangrove forests and salt-marshes due to shallow subsidence and sedimentation (<http://www.pwrc.usgs.gov/set/>). SET have been installed in the mangrove forest by NIWA and Environment Waikato to provide basic information for research and management of mangrove forests.

7. Acknowledgements

We thank Mark Williams, Clint Prior, Jacky Hovens and Sarah Orchard (Environment Waikato GIS Group) for analysis of the historical aerial photographs. Mark Williams also prepared the images of the historical changes in mangrove habitat used in this report. Rick Liefing (formerly Environment Waikato) initiated the study. We are grateful to Bill Brownell (Ecoquest Education Foundation) for his support of this project. Thanks to Mrs Allyson McAulay for site access and for Fig. 4.4. Dr Catherine Lovelock (Centre for Marine Studies, University of Queensland) provided the canopy-height data (Fig. 5.1). Andrew Swales thanks Dr Samuel Bentley (Memorial University of Newfoundland) for helpful discussions regarding interpretation of core LC-6. Additional radioisotope analyses of the sediment cores and monitoring of ^{210}Pb atmospheric deposition were funded by NIWA's FRST-funded *Effects-Based Protection and Management of Aquatic Ecosystems* (CO1X0307).

8. References

- Allen, J.R.L. (1990). Salt-marsh growth and stratification: A numerical model with special reference to the Severn Estuary, southwest Britain. *Marine Geology* 95: 77–96.
- Augustinus, P.G.E.F. (1980). “Actual development of the chenier coast of Suriname (South America),” *Sedimentary Geology* 26: 91–113.
- Beaglehole, J.C. (1968). The journals of Captain James Cook on his voyages of discovery. *The voyage of Endeavour 1768–1771*. Cambridge University Press.
- Beard, C.M. (2006). Physiological constraints on the latitudinal distribution of the mangrove *Avicennia marina* (Forsk) Vierh. Subsp *australasica* (Walp.) J. Everett (*Avicenniaceae*) in New Zealand. Unpublished Ph.d. thesis, University of Waikato, 229 p.
- Bell, R.G.; Oldman, J.W.; Stephens, S.A. (2004). Recent applications of 3D wind-driven circulation modeling to a semi-enclosed sea: Hauraki Gulf, New Zealand. In: Spaulding, M.L. (Ed.), *Estuarine & Coastal Modelling*. Proceedings of the Eighth International Conference, Monterey, Nov. 3-5, 2003. American Society of Civil Engineers (ASCE), Reston, Virginia. p. 288–307.
- Bell, R.G.; Goodhue, N. (2007). Mean level of the sea at Tararu: 1993–2006. NIWA Client Report HAM2007-084 prepared for Environment Waikato.
- Benoit, G.; Rozan, T.F.; Patton, P.C.; Arnold, C.L. (1999). Trace metals and radionuclides reveal sediment sources and accumulation rates in Jordan Cove, Connecticut. *Estuaries* 22(1): 65–80.
- Black, K.P.; Bell, R.G.; Oldman, J.O.; Carter, G.S.; Hume, T.M. (2000). Features of 3-dimensional barotropic and baroclinic circulation in the Hauraki Gulf, New Zealand. *NZ Journal of Marine & Freshwater Research* 34(1): 1–28.
- Brinkman, R.M.; Massel, S.R.; Ridd, P.V.; Furukawa, K. (1997). Surface wave attenuation in mangrove forests. *Proceedings of Australasian Coasts & Ports Conference, Christchurch, Vol. 2*: 941–946.
- Bromley, R.G. (1996). Trace fossils: biology, taphonomy and applications, second edition. Chapman and Hall, London, 361 p.

- Brownell, B. (2004). Muddy Feet: Firth of Thames RAMSAR site update 2004. Ecoquest Education Foundation, Kaiaua, New Zealand, 198 p.
- Burns, B.R. and Ogden, J. (1985). The demography of the temperate mangrove (*Avicennia marina* (Forsk.) Vierh.) at its southern limit in New Zealand. *Australian Journal of Ecology* 10: 125-133.
- Cahoon, D.; Day, J.W.; Reed, D.J. (1999). "The influence of surface and shallow subsurface soil processes on wetland elevation: a synthesis," *Current topics in wetland biogeochemistry* 3: 72-88.
- Chick, L.M.; de Lange, W.P.; Healy, T.R. (2001). Potential tsunami hazard associated with the Kerepehi Fault, Firth of Thames, New Zealand. *Natural Hazards* 24: 309-318.
- Clarke, P.J. and Myerscough, P.J. (1993). The intertidal distribution of the grey mangrove (*Avicennia marina*) in southeastern Australia: The effects of physical conditions, interspecific competition, and predation on propagule establishment and survival. *Australian Journal of Ecology* 18: 307-315.
- Crisp, P.; Daniel, L.; Tortell, P. (1990). Mangroves in New Zealand – trees in the tide. GP Books, Wellington, 69 p.
- Dahdouh-Guebas, F.; Jayatissa, L.P.; Di Nitto, D.; Bosire, J.O.; Lo Seen, D.; Koedam, N. (2005). How effective were mangroves as a defence against the recent tsunami? *Current Biology* 15(12): R443-R447.
- de Lange, P.J.; Lowe, D.J. (1990). History of vertical displacement of the Kerepehi fault at Kopouatai bog, Hauraki lowlands, New Zealand, since c. 10,700 years ago, *New Zealand Journal of Geology and Geophysics* 33: 277-284.
- de Lange, W.P.; de Lange, P.J. (1994). An appraisal of factors controlling the latitudinal distribution of mangrove (*Avicennia marina* var. *resinifera*) in New Zealand. *Journal of Coastal Research* 10(3): 539-548.
- de Lange, W.P.; Healy, T.R. (2001). Tsunami hazard for the Auckland region and Hauraki Gulf, New Zealand. *Natural Hazards* 24: 267-284.

- Deng, Y.; Horrocks, M.; Ogden, J.; Anderson, S. (2006). Modern pollen-vegetation relationships along transects on the Whangapoua Estuary, Great Barrier Island, northern New Zealand. *Journal of Biogeography* 33: 592-608.
- Duder, J.N.; Crawford, S.A.; Reinen-Hamill, R.; Jensen, C.P. (1999). Design and construction of inundation protection for Moanataiari subdivision, Thames. Proceedings of 1999 IPENZ Technical Conference, Auckland, Published by the Institution of Professional Engineers New Zealand.
- Duke, N.C.; Ball, M.C.; Ellison, J.C. (1998). Factors influencing biodiversity and distributional gradients in mangroves. *Global Ecology and Biogeography Letters* 7(1): 27-47.
- Ellis, J.; Nicholls, P.; Craggs, R.; Hofstra, D. & Hewitt, J. (2004). Effects of terrigenous sedimentation on mangrove physiology and associated macrobenthic communities. *Marine Ecology Progress Series* 270: 71-82.
- French, J.R. (1993). Numerical simulation of vertical marsh growth and adjustment to accelerated sea-level rise, North Norfolk, U.K. *Earth Surface Processes and Landforms* 18: 63-81.
- Furukawa, K.; Wolanski, E. & Mueller, H. (1997). Currents and sediment transport in mangrove forests. *Estuarine, Coastal and Shelf Science* 44: 301-310.
- GeoEnvironmental Consultants (2005). Tsunami Overview Study. Auckland Regional Council Report GEO2005/20060, 35 p.
- Goff, J. (1997). A chronology of natural and anthropogenic influences on coastal sedimentation, New Zealand. *Marine Geology* 138: 105-117.
- Goring, D.G. (2003). Analysis of Tararu sea-level record: 1992-2003. NIWA Client Report CHC2003-062 prepared for Environment Waikato. June 2003, 34 p.
- Goldberg, E.D.; Kiode, M. (1962). Geochronological studies of deep sea sediments by the ionium/thorium method. *Geochimica et Cosmochimica Acta* 26: 417-450.
- Gorman, R.M.; Heydenrych, C. (2004). Hauraki Gulf wave climate simulation. NIWA Consultancy Report HAM2004-092 prepared for the Auckland Regional Council, 115 p.

- Greig, M.J.; Proctor, R. (1989). A numerical model of the Hauraki Gulf, New Zealand. *New Zealand Journal of Marine and Freshwater Research* 22: 379–390.
- Guinasso, N.L. Jr.; Schink, D.R. (1975). Quantitative estimates of biological mixing rates in abyssal sediments. *Journal of Geophysical Research* 80: 3032–3043.
- Hannah, J. (2004). An updated analysis of long-term sea level change in New Zealand. *Geophysical Research Letters* 31(L03307): 1-4.
- Harris, T.F.W. (1993). The Mahurangi System. Prepared for Environment and Planning Division, Auckland Regional Council, 120 p.
- Hauraki Plains Gazette (1938). Sea bursts stopbank: Plains invaded. News article in Hauraki Plains Gazette, Friday May 6, 1938.
- HCBRWB (1978). Preliminary report on the storm July 18th to 19th 1978. File report by R.W. Harris, Chief Engineer, Hauraki Catchment Board & Regional Water Board. 7 p.
- Healy, T.R. (2002). *Muddy coasts of mid-latitude oceanic islands on an active plate margin – New Zealand*, p 347–374. In Healy, T. Yang, J.-A. Healy, (eds.) *Muddy coasts of the world: processes, deposits and function*.
- Hochstein, M.P.; Nixon, I. M. (1979). Geophysical study of the Hauraki Depression, North Island, New Zealand, *New Zealand Journal Geology & Geophysics* 22: 1–19.
- Horrocks, M.; Coulson, S.A.; Walsh, K.A.J. (1998). Forensic palynology: variation in the pollen content of soil surface samples. *Journal of Forensic Sciences* 43: 320-323.
- Horrocks, M.; Ogden, J.; Nichol, S.L.; Alloway, B.V.; Sutton, D.G. (2000). A Late Quaternary palynological and sedimentological record from two coastal swamps at southern Kaitoke, Great Barrier Island. *Journal of the Royal Society of New Zealand* 30: 49-68.
- Horrocks, M.; Ogden, J.; Nichol, S.L.; Alloway, B.V.; Sutton, D.G. (2000). Palynology, sedimentology and environmental significance of Holocene swamps at northern Kaitoke, Great Barrier Island, New Zealand. *Journal of the Royal Society of New Zealand* 30: 27-47.

- Horrocks, M.; Nichol, S.L.; Gregory, M.R.; Creese, R.; Augustinus, P.C. (2001). A Holocene pollen and sediment record of Whangape Harbour, Far Northern New Zealand. *Journal of the Royal Society of New Zealand* 31: 411-424.
- Hume, T.M. (1979). Factors contributing to coastal erosion on the east coast of Northland during July 1978. Water and Soil Division, Ministry of Works and Development, Auckland, 25 p.
- Hume, T.M.; McGlone, M.S. (1986). Sedimentation patterns and catchment use change recorded in the sediments of a shallow tidal creek, Lucas Creek, Upper Waitemata Harbour, New Zealand. *New Zealand Journal of Marine and Freshwater Research* 20: 677-687.
- Hume, T.M.; Dahm, J. (1992). An investigation of the effects of Polynesian and European land use on sedimentation in Coromandel estuaries. DSIR Marine and Freshwater Consultancy Report 6104.
- IPCC (2007). Climate Change 2007: The Physical Science Basis. Contribution of Working Group I to the Fourth Assessment Report of the Intergovernmental Panel on Climate Change [Solomon, S.; D. Qin; M. Manning; Z. Chen; M. Marquis; K.B. Averyt; M. Tignor and H.L. Miller (eds.)]. Cambridge University Press, Cambridge, United Kingdom and New York, NY, USA.
- Janssen-Stelder, B.M.; Augustinus, P.G.E.F.; van Santen, W.A.C. (2002). Sedimentation in a coastal mangrove system, Red River Delta, Vietnam. In Winterwerp, J.C., and Kranenberg, C. (eds.), *Fine Sediment Dynamics in the Marine Environment*, Proceedings in Marine Science 5. Elsevier, Amsterdam. pp. 455-467.
- Kristensen, E. & Alongi, D.M. (2006). Control by fiddler crab (*Uca vocans*) and plant roots (*Avicennia marina*) on carbon, iron, and sulphur biogeochemistry in mangrove sediment. *Limnology and Oceanography* 51(4): 1557-1571.
- Massel, S.R.; Furukawa, K.; Brinkman, R.M. (1999). Surface wave propagation in mangrove forests. *Fluid Dynamics Research* 24: 219-249.
- Matthews, K.M. (1989). Radioactive fallout in the South Pacific a history. Part 1. Deposition in New Zealand. Report NRL 1989/2. National Radiation Laboratory, Christchurch, New Zealand.

- Mehta, A.J. (2002). "Mud-shore dynamics and controls," p 19–60. *In*: Healy, T., Yang, J.-A. Healy, (eds.) *Muddy coasts of the world: processes, deposits and function*.
- McKee, K.L.; Cahoon, D.R.; Feller, I.C. (2007). Caribbean mangroves adjust to rising sea level through biotic controls on change in soil elevation. *Global Ecology and Biogeography*, DOI: 10.1111/j.1466-8238.2007.00317.x
- McLeod, E.; Salm, R. (2006). *Managing mangroves for resilience to climate change*. IUCN Resilience Science Group Working Paper Series No. 2, Gland Switzerland, 64 p.
- Moore, P.D.; Webb, J.A.; Collinson, M.E. (1991). *Pollen Analysis, 2nd Edition*. Blackwell, London.
- Mildenhall, D.C. (1994). Early to Mid Holocene pollen samples containing mangrove pollen from Sponge Bay, East Coast, North Island, New Zealand. *Journal of the Royal Society of New Zealand* 24: 210-230.
- Morrisey, D.; Beard, C.; Morrison, M.; Craggs, R.; Lowe, M. (2007). *The New Zealand mangrove: review of the current state of knowledge*. NIWA Client Report HAM2007-052. ARC Technical Publication TP325, 165 p.
- Muller, J. (1964). A palynological contribution to the history of the mangrove vegetation in Borneo. *In*: Cranwell, L.M. (ed). *Ancient Pacific Floras*. University of Hawaii Press, Honolulu, pp. 33-42.
- Naish, T.R. (1990). *Late Holocene mud sedimentation and diagenesis in the Firth of Thames: Bentonites in the making*. Unpublished MSc. Thesis, Earth Sciences Department, University of Waikato, New Zealand, 154 p.
- Ogden, J.; Deng, Y.; Horrocks, M.; Nichol, S.; Anderson, S. (2006). Sequential impacts of Polynesian and European settlement on vegetation and environmental processes recorded in sediments at Whangapoua Estuary, Great Barrier Island, New Zealand. *Regional Environmental Change* 6: 25-40.
- Othman, M.A. (1994). Value of mangroves in coastal protection. *Hydrobiologia* 285(1–3): 277–282.

- Park, S. (2004). Aspects of mangrove distribution and abundance in Tauranga Harbour. Environment Bay of Plenty Publication 2004/16. ISSN 1175-9372, 40 p.
- Phillips, C. (2000). Waihou Journeys. The archaeology of 400 years of Maori settlement. Auckland University Press.
- Phuoc, V.L.H.; Massel, S.R. (2006). Wave propagation in non-uniform mangrove forests in water of arbitrary depth. *Geophysical Research Abstracts* 8, No. 00562, European Geoscience Union 06.
- Pocknall, D.T.; Gregory, M.R.; Greig, D.A. (1989). Palynology of core 80/20 and its implications for understanding Holocene sea level changes in the Firth of Thames, New Zealand. *Journal of the Royal Society of New Zealand* 19(2): 171–179.
- Postma, H. (1961). Transport and accumulation of suspended matter in the Dutch Wadden Sea. *Netherlands Journal of Sea Research* 1: 148-190.
- Ray, D.E.; Palmer, G.N. (1993). Management of coastal flood hazards in the Waikato region, New Zealand. Proceedings of 11th Australasian Conference on Coastal & ocean Engineering, Townsville. National Conference Publication No. 93/4, The Institute of Engineers, Australia, Vol. 2: 495–500.
- Reineck, H.E. & Singh, I.B. (1980). “Depositional Sedimentary Environments, second revised edition,” Springer-Verlag, Berlin.
- Roth, L.C. (1992). Hurricanes and mangrove regeneration: Effects of Hurricane Joan , October 1988, on the vegetation of Isla del Venado, Bluefields, Nicaragua. *Biotropica* 24(3): 375–384.
- Ritchie, J.C. & McHenry, J.R. (1989). Application of radioactive fallout cesium-137 for measuring soil erosion and sediment accumulation rates and patterns: A review with bibliography. Hydrology Laboratory, Agriculture Research Service, U.S. Department of Agriculture, Maryland.
- Robbins, J.A.; Edgington, D.N. (1975). Determination of recent sedimentation rates in Lake Michigan using ²¹⁰Pb and ¹³⁷Cs. *Geochimica et Cosmochimica Acta* 39: 285–304.
- Schwarz, A.M. (2002). The role of nutrients in contributing to mangrove expansion. NIWA Client Report HAM2002-051, NIWA Hamilton

- Sharma, K.; Gardner, L.R.; Moore, W.S.; Bollinger, M.S. (1987). Sedimentation and bioturbation in a saltmarsh revealed by ^{210}Pb , ^{137}Cs , and ^7Be studies. *Limnology and Oceanography* 32(2): 313–326.
- Smith, T.J. III. (1992). “Forest structure,” In Robertson, A.I., and Alongi, D.M. (eds.), *Tropical Mangrove Ecosystems*, Coastal and Estuarine Studies, 41. American Geophysical Union. Washington DC. pp. 101-136.
- Sommerfield, C.K.; Nittrouer, C.A. & Alexander, C.R. (1999). ^7Be as a tracer of flood sedimentation on the Northern California margin. *Continental Shelf Research* 19: 335–361.
- Swales, A.; Hume, T.M.; Oldman, J.W.; Green, M.O. (1997). Holocene sedimentation and recent human impacts in a drowned-valley estuary, p 895–900. In J. Lumsden (ed.), Proceedings of the 13th Australasian Coastal and Ocean Engineering Conference, Centre for Advanced Engineering, University of Canterbury, Christchurch, New Zealand.
- Swales, A.; Williamson, R.B.; Van dam, L.F.; Stroud, M.J. (2002). Reconstruction of urban stormwater contamination of an estuary using catchment history and sediment profile dating. *Estuaries* 25(1): 43–56.
- Swales, A.; Hume, T.M.; McGlone, M.S.; Pilvio, R.; Ovenden, R.; Zviguina, N.; Hatton, S.; Nicholls, P.; Budd, R.; Hewitt, J.; Pickmere, S.; Costley, K. (2002b). Evidence for the physical effects of catchment sediment runoff preserved in estuarine sediments: Phase II (field study). ARC Technical Publication 221 NIWA Client Report HAM2002-067.
- Swales, A.; Bentley, S.J.; Lovelock, C.; Bell, R.G. (2007). Sediment processes and mangrove-habitat expansion on a rapidly-prograding muddy coast, New Zealand. Proceedings of the Sixth International Symposium on Coastal Engineering and Science of Coastal Sediment Processes (New Orleans, May 2007). *Coastal Sediments '07* (Volume 2): 1441–1454.
- Wells, J.T. & Coleman, J.M. (1981). “Physical processes and fine-grained sediment dynamics, coast of Surinam, South America,” *Journal of Sedimentary Petrology* 51: 1053–1068.
- Wilmshurst, J.; Eden, D.N.; Frogatt, P.C. (1999). Late Holocene forest disturbance in Gisborne, New Zealand. *New Zealand Journal of Botany* 37: 523–540.

- Wise, S. (1977). The use of radionuclides ^{210}Pb and ^{137}Cs in estimating denudation rates and in soil erosion measurement. Occasional Paper No. 7 University of London, King's College, Department of Geography, London.
- Woodroffe, C.D.; Curtis, R.J.; McLean, R.F. (1983). "Development of a chenier plain, Firth of Thames, New Zealand," *Marine Geology* 53, 1–22.
- Woodroffe, C.D. (2002). Coasts: form, process and evolution. Cambridge University Press, Cambridge, U.K. 623 p.
- Young, B.M.; Harvey, L.E. (1996). A spatial analysis of the relationship between mangrove (*Avicennia marina* var. *australasica*) physiognomy and sediment accretion in the Hauraki Plains, New Zealand. *Estuarine, Coastal and Shelf Science* 42: 231–246.

9. Appendix One: Dating of estuarine sediments

9.1 Overview

Radioisotopes, such as caesium-137 (^{137}Cs , $\frac{1}{2}$ -life 30 years) and lead-210 (^{210}Pb , $\frac{1}{2}$ -life 22.3 years), and plant pollen can be used to reconstruct the recent sedimentation history of an estuary.

Dating of estuarine sediments using independent methods offsets the limitations of any one approach. This is particularly important when interpreting sediment profiles from lakes and estuaries, given the confounding effects of physical and biological mixing (Robbins and Edgington, 1975; Sharma et al. 1987; Alexander et al. 1993; Valette-Silver, 1993; Benoit et al. 1999). A description of the various methods of dating sediments follows.

The S.I. unit of radioactivity used in this study is the Becquerel (Bq), which is equivalent to one radioactive disintegration per second.

9.2 ^{137}Cs dating

^{137}Cs was introduced to the environment by atmospheric nuclear weapons tests in 1953, 1955–1956 and 1963–1964. Peaks in annual ^{137}Cs deposition corresponding to these dates are the usual basis for dating sediments (Wise, 1977; Ritchie and McHenry, 1989). Although direct atmospheric deposition of ^{137}Cs into estuaries is likely to have occurred, ^{137}Cs is also incorporated into catchment soils, which are subsequently eroded and deposited in estuaries (Fig. 8.1). In New Zealand, ^{137}Cs deposition was first detected in 1953 and its annual deposition was been measured at several locations until 1985. Annual ^{137}Cs deposition can be estimated from rainfall using known linear relationships between rainfall and Strontium-90 (^{90}Sr) and measured $^{137}\text{Cs}/^{90}\text{Sr}$ deposition ratios (Matthews, 1989). Experience in Auckland estuaries shows that ^{137}Cs profiles measured in estuarine sediments bear no relation to the record of annual ^{137}Cs deposition (i.e., 1955–1956 and 1963–1964 ^{137}Cs -deposition peaks absent), but rather preserve a record of direct and indirect (i.e., soil erosion) atmospheric deposition since 1953 (Swales et al. 2002b). The maximum depth of ^{137}Cs occurrence in sediment cores (corrected for sediment mixing) is taken to coincide with the year 1953, when ^{137}Cs deposition was first detected in New Zealand. We assume that there is a negligible delay in initial atmospheric deposition of ^{137}Cs in estuarine sediments (e.g., ^{137}Cs scavenging by suspended particles) whereas there is likely to have been a time-lag (i.e., < 1 yr) in ^{137}Cs inputs to estuaries from topsoil erosion, which would coincide with the occurrence of floods.

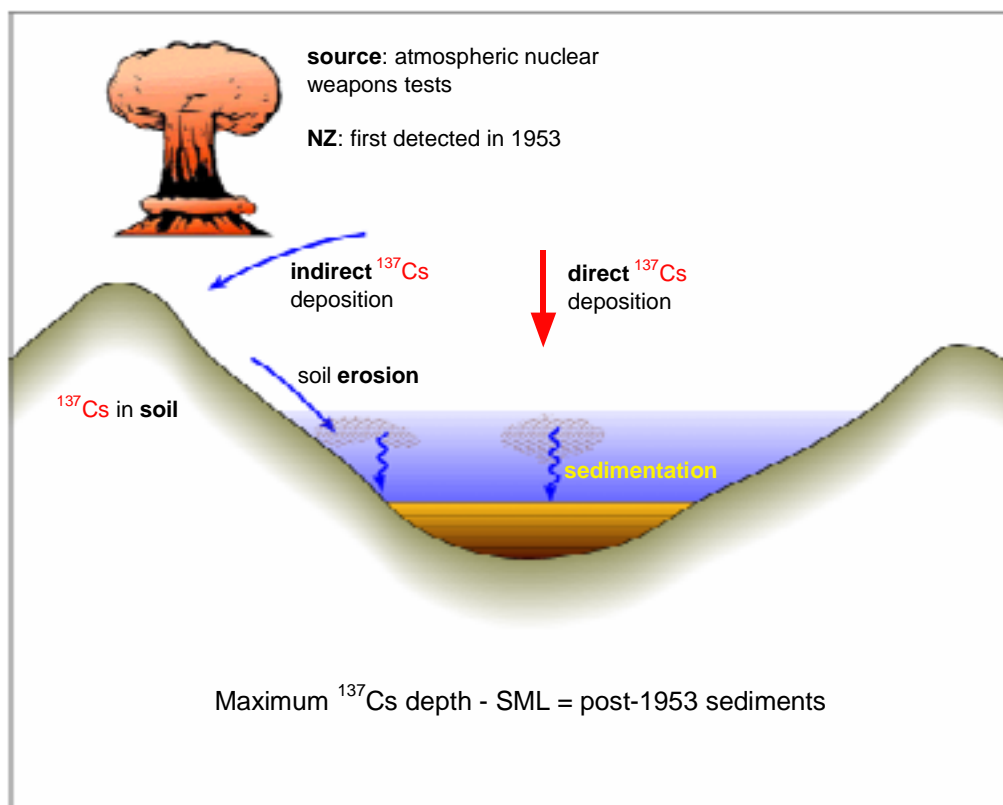


Figure 8.1: ^{137}Cs pathways to estuarine sediments.

If a surface mixed layer (SML) is evident in a core, as shown by an x-ray image and/or a tracer profile (e.g., ^7Be , ^{210}Pb) then ^{137}Cs is likely to have been rapidly mixed through the SML. Therefore, to calculate time-averaged sedimentation rates, the maximum depth of ^{137}Cs occurrence is reduced by the maximum depth of the SML.

Uncertainty in the maximum depth of ^{137}Cs results from: (1) the depth interval between sediment samples and (2) minimum detectable concentration of ^{137}Cs , which is primarily determined by sample size and counting time. The 1963–1964 ^{137}Cs deposition peak was about five-times than the deposition plateau that occurred between 1953 and 1972. Thus, depending on the sample size, there is uncertainty in the age of the maximum ^{137}Cs depth (i.e., 1953–1963). To reduce this uncertainty, we have maximised the sample mass that is analysed (section 3).

9.3 ^{210}Pb dating

^{210}Pb (half-life 22.3 yr) is a naturally occurring radioisotope that has been widely applied to dating recent sedimentation (i.e., last 150 yrs) in lakes, estuaries and the sea (Fig. 8.2). ^{210}Pb is an intermediate decay product in the uranium-238 (^{238}U) decay

series and has a radioactive decay constant (k) of 0.03114 yr^{-1} . The intermediate parent radioisotope radium-226 (^{226}Ra , half-life 1622 years) yields the inert gas radon-222 (^{222}Rn , half-life 3.83 days), which decays through several short-lived radioisotopes to produce ^{210}Pb . A proportion of the ^{222}Rn gas formed by ^{226}Ra decay in catchment soils diffuses into the atmosphere where it decays to form ^{210}Pb . This atmospheric ^{210}Pb is deposited at the earth surface by dry deposition or rainfall. The ^{210}Pb in estuarine sediments has two components: supported ^{210}Pb derived from *in situ* ^{222}Rn decay (i.e., within the sediment column) and an unsupported ^{210}Pb component derived from atmospheric fallout. This unsupported ^{210}Pb component of the total ^{210}Pb concentration in excess of the supported ^{210}Pb value is estimated from the ^{226}Ra assay (see below). Some of this atmospheric unsupported ^{210}Pb component is also incorporated into catchment soils and is subsequently eroded and deposited in estuaries. Both the direct and indirect (i.e., soil inputs) atmospheric ^{210}Pb input to receiving environments, such as estuaries, is termed the unsupported or excess ^{210}Pb .

The concentration profile of unsupported ^{210}Pb in sediments is the basis for ^{210}Pb dating. In the absence of atmospheric (unsupported) ^{210}Pb fallout, the ^{226}Ra and ^{210}Pb in estuary sediments would be in radioactive equilibrium, which results from the substantially longer ^{226}Ra half-life. Thus, the ^{210}Pb concentration profile would be uniform with depth. However, what is typically observed is a reduction in ^{210}Pb concentration with depth in the sediment column. This is due to the addition of unsupported ^{210}Pb directly or indirectly from the atmosphere that is deposited with sediment particles on the bed. This unsupported ^{210}Pb component decays with age ($k = 0.03114 \text{ yr}^{-1}$) as it is buried through sedimentation. In the absence of sediment mixing, the unsupported ^{210}Pb concentration decays exponentially with depth and time in the sediment column. The validity of ^{210}Pb dating rests on how accurately the ^{210}Pb delivery processes to the estuary are modelled, and in particular the rates of ^{210}Pb and sediment inputs (i.e., constant versus time variable).

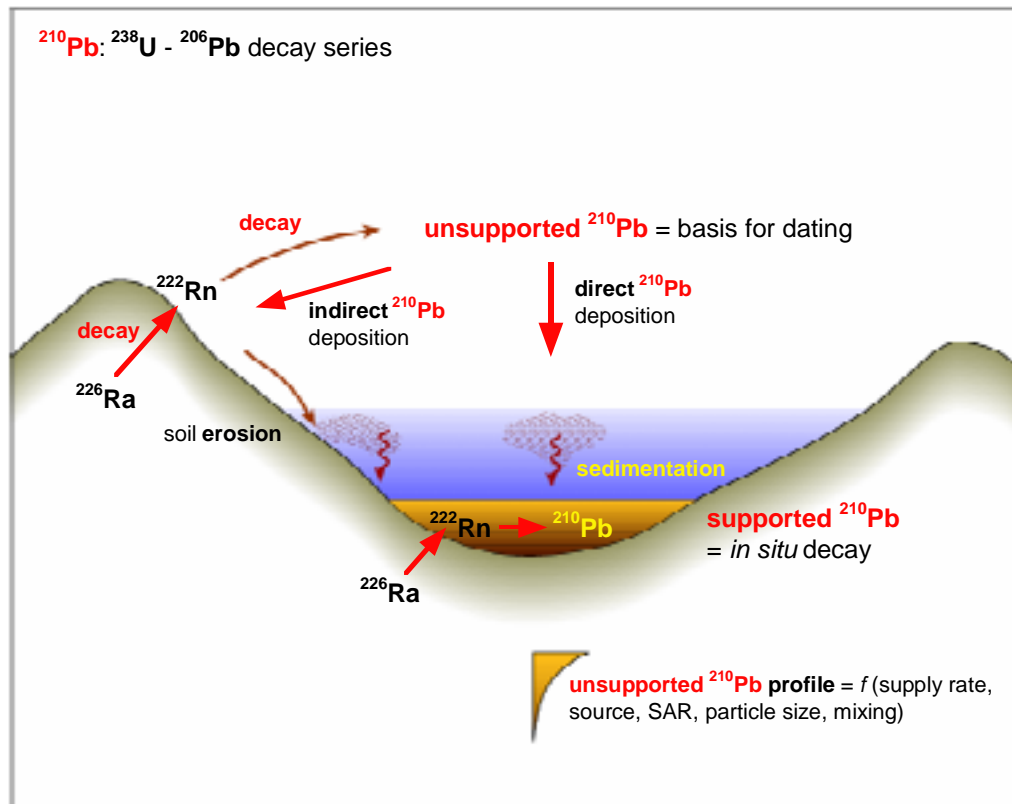


Figure 8.2: ^{210}Pb pathways to estuarine sediments.

9.3.1 Pollen dating

Historical landcover changes, such as catchment deforestation, establishment of pasture, plantation forestry or urbanisation, alter the composition of the pollen assemblage. Pollen is delivered to estuaries by direct atmospheric deposition and by eroded catchment soil. Thus, changes in the abundances of plant pollen in estuarine sediments can be used for dating deposits if the history of catchment landcover change is known. The uncertainty in dating sediment cores using pollen largely depends on two factors: (1) the degree of *in situ* sediment mixing, the efficiency of which declines as sedimentation rate increase and (2) the time lag between the initial introduction of new plant species and the production of sufficient pollen to be detectable in the stratigraphic record. The time lag for pollen production varies between plant species. New Zealand native trees take up to 50 years to reach full reproductive maturity whereas the introduced pine, *Pinus radiata*, develops a substantial pollen rain within 10 years. Grasses, weeds and other short-lived plants flower immediately and enter the stratigraphic record quickly. We assume a pollen dating uncertainty of ~10 yr, based on the time lag for pine pollen production and detection in estuarine sediments.

In the North Island, terrestrial pollen assemblages associated with several historical time periods have been identified in estuarine cores: (1) pre-human indigenous forest; (2) Maori settlement (1350 AD \pm 100 years) identified by indigenous forest with bracken and charcoal increasing; (3) European settlement (mid-1800s onwards) with a rapid reduction in native forest species; (4) Modern sediments (typically post-1945) distinguished by a rapid rise in exotic grass and tree species (e.g., *Pinus*).

Pollen grains and spores (palynomorphs) are produced in huge numbers by conifers, flowering plants, ferns, and fern allies. Most palynomorphs are in the size range 5–120 μ m, and thus can be easily transported by wind or water. In the presence of oxygen and moisture the cytoplasm decays rapidly, but the tough, decay-resistant outer wall tends to persist, although it will eventually break down. If sediments are water-saturated, and thus oxygen levels are reduced to very low levels, the outer walls can persist indefinitely. A cubic centimetre of most soils and estuarine sediments will contain thousands of pollen grains and spores. Palynomorphs (i.e., pollen and spores) are most often identified to a familial or generic level, although a substantial number can be attributed to one or several closely related species.

There are three main pathways by which palynomorphs are incorporated into the estuarine stratigraphic record (Fig. 8.3):

- airborne palynomorphs may fall directly onto the estuary sediment (low tide) or the overlying water mass (high tide);
- palynomorphs drop directly onto the surface of catchment soils and waterways and are delivered to the estuary by fluvial processes;
- palynomorphs accumulated in catchment soils, rocks and other sediments are reworked (10^1 – 10^6 yr after initial deposition) and eroded and transported by fluvial processes to the estuary.

The final palynomorph assemblage will always reflect varying proportions of these three pathways. Airborne palynomorphs suffer no corrosion and little breakage before incorporation in sediments. Palynomorphs reworked along waterways will show some corrosion or breakage if they spend time in sediments along stream-banks and beds where bacteria are active. Soils, however, have a dramatic effect on palynomorphs. Fern spores are highly resistant to corrosion, but flowering plant pollen is highly susceptible and conifers have intermediate resistance to corrosion. The longer a collection of palynomorphs is in the soil, the more fern spores and, in particular, tree-fern spores will dominate. A well-drained (aerated) soil will lose nearly all

palynomorphs except for extensively corroded tree-fern spores. Thus, an estuarine sediment dominated by tree-fern spores is nearly always the result of a pollen source dominated by eroded catchment soils.

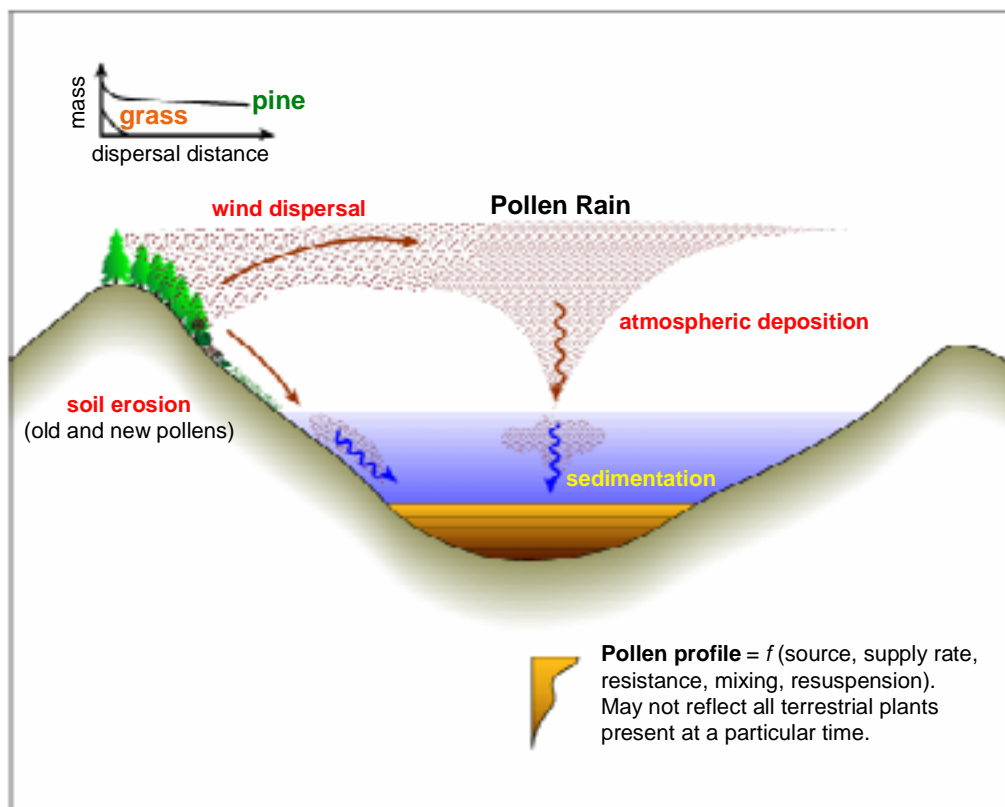


Figure 8.3: Pollen pathways to estuarine sediments.

Bracken (*Pteridium esculentum*) spores are produced in large numbers, and are wind-dispersed and corrosion-resistant. In the Auckland region, bracken and scrub covered large areas after Maori settlement and forest clearance. Soils rich in bracken spores can continue to provide a steady influx of bracken spores to estuaries even when bracken has been nearly eliminated from the local area (Wilmshurst et al. 1999). In the present study, bracken spores are also found in sediment cores.

Pine (*Pinus*) pollen is probably the most abundantly produced and widely distributed of all types (exotic and native) in the New Zealand flora. Slicks of yellow pollen that are sometimes noticeable after rain on suburban streets are often derived from pine plantations many kilometres distant. Pine trees begin to flower as soon as five years after planting. However, pine pollen production depends on tree size and the distance pollen is dispersed is proportional to the height above the ground at which it is released. Pollen production from a pine plantation therefore gradually increases over

time, reflecting the number of saplings coming into flower (as all the trees are not planted at once), tree height and the foliage coverage. Pollen contributions from a plantation should first become apparent after 5 years, but the full effect is delayed until ~10 years after planting. In interpreting pine pollen profiles, it is reasonable to assume a typical sigmoidal growth curve, with an initial period of rapid increase followed by a decline in growth rate that eventually plateaus as maturity is reached. This sigmoidal growth pattern is mirrored in the pollen production, with an initial rapid increase, which eventually stabilises to roughly uniform level of year-to-year pollen production. This pattern has been observed in a regional study of sedimentation in Auckland estuaries (Swales et al. 2002b).

9.4 Sediment accumulation rates (SAR)

Sedimentation rates calculated from cores are **net average sediment accumulation rates (SAR), which are usually expressed as mm yr⁻¹**. These SAR are net values because cores integrate the effects of all processes, which influence sedimentation at a given location. At short time scales (i.e., seconds–months), sediment may be deposited and then subsequently resuspended by tidal currents and/or waves. Thus, over the long term, sedimentation rates derived from cores represent net or cumulative effect of potentially many cycles of sediment deposition and resuspension. However, less disrupted sedimentation histories are found in depositional environments where sediment mixing due to physical processes (e.g., resuspension) and bioturbation is limited. The effects of bioturbation on sediment profiles and dating resolution reduce as SAR increase (Valette-Silver, 1993).

Net sedimentation rates also mask the fact that sedimentation is an episodic process, which largely occurs during catchment floods, rather than the continuous gradual process that is implied. In large estuarine embayments, such as the Firth, mudflat sedimentation is also driven by wave-driven resuspension events. Sediment eroded from the mudflat is subsequently re-deposited elsewhere in the estuary.

Although sedimentation rates are usually expressed as a sediment thickness deposited per unit time (i.e., mm yr⁻¹) this statistic does not account for changes in dry sediment mass with depth in the sediment column due to compaction. Typically, sediment density ($\rho = \text{g cm}^{-3}$) increases with depth and therefore some workers prefer to calculate dry mass accumulation rates per unit area per unit time (g cm⁻² yr⁻¹). These data can be used to estimate the total mass of sedimentation in an estuary (tonnes yr⁻¹) (e.g., Swales et al. 1997). However, the effects of compaction can be offset by changes in bulk sediment density reflecting layering of low-density mud and higher-density sand deposits. Furthermore, the significance of a SAR expressed as mm yr⁻¹ is

more readily grasped than a dry-mass sedimentation rate in $\text{g cm}^{-3} \text{ yr}^{-1}$. For example, the rate of estuary aging due to sedimentation (mm yr^{-1}) can be directly compared with the local rate of sea level rise.

9.5 SAR from ^{210}Pb dating

In this study, we calculate time-averages sediment accumulation rates (SAR) from the unsupported ^{210}Pb ($^{210}\text{Pb}_{\text{us}}$) concentration profiles for cores LC-3 to LC-12. The rate of $^{210}\text{Pb}_{\text{us}}$ concentration decrease with depth can be used to calculate a net sediment accumulation rate. The $^{210}\text{Pb}_{\text{us}}$ concentration at time zero (C_0 , Bq kg^{-2}), declines exponentially with age (t):

$$C_t = C_0 e^{-kt} \quad \text{Eq. 1}$$

Assuming that within a finite time period, sedimentation (S) or SAR is constant then $t = z/S$ can be substituted into Eq. 1 and by re-arrangement:

$$\frac{\ln\left[\frac{C_t}{C_0}\right]}{z} = -k/S \quad \text{Eq. 2}$$

Because $^{210}\text{Pb}_{\text{us}}$ concentration decays exponentially and assuming that sediment age increases with depth, a vertical profile of natural $\log(C)$ should yield a straight line of slope $b = -k/S$. We fitted a linear regression model to natural-log transformed ^{210}Pb concentration data to calculate b . The sedimentation rate over the depth of the fitted data is given by:

$$S = -(k)/b \quad \text{Eq. 3}$$

An advantage of this method is that the sedimentation rate is based on the entire ^{210}Pb profile rather than a single layer, as is the case for ^{137}Cs . Furthermore, if the pollen or ^{137}Cs tracer is present at the bottom of the core then the estimated SAR is a minimum value. The SAR found by the ^{210}Pb method can also be used to estimate the residence time (R) of sediment particles in the surface mixed layer (SML) before they are removed by burial. For example, given an SML (L) depth of 40 mm and S of 2 mm yr^{-1} then $R = L/S = 20$ years. Although this greatly simplifies the process (i.e., the likelihood of particle mixing reduces with depth in the SML), this approach provides a useful measure of the relative effect of sediment mixing between cores, sub-environments and estuaries.

9.6 Sediment Mixing

Biological and physical processes, such as the burrowing and feeding activities of animals and/or sediment resuspension by waves (Fig. 8.4), mix the upper sediment column (Bromley, 1996). As a result, sediment profiles are modified and this limits the temporal resolution of dating. Various mathematical models have been proposed to take into account the effects of bioturbation on ^{210}Pb concentration profiles (e.g., Guinasso and Schink, 1975). Biological mixing has been modelled as a one-dimensional particle-diffusion process (Goldberg and Kiode, 1962) and this approach is based on the assumption that the sum effect of ‘random’ biological mixing is integrated over time. In estuarine sediments exposed to bioturbation, the depth profile of unsupported ^{210}Pb typically shows a two-layer form, with a surface layer of relatively constant unsupported ^{210}Pb concentration overlying a zone of exponential decrease (Figs. 5.3i–j). In applying these types of models, the assumption is made that the mixing rate (i.e., diffusion co-efficient) and mixing depth (i.e., surface-mixed layer, SML) are uniform in time. The validity of this assumption usually cannot be tested, but changes in bioturbation process could be expected to follow changes in benthic community composition.

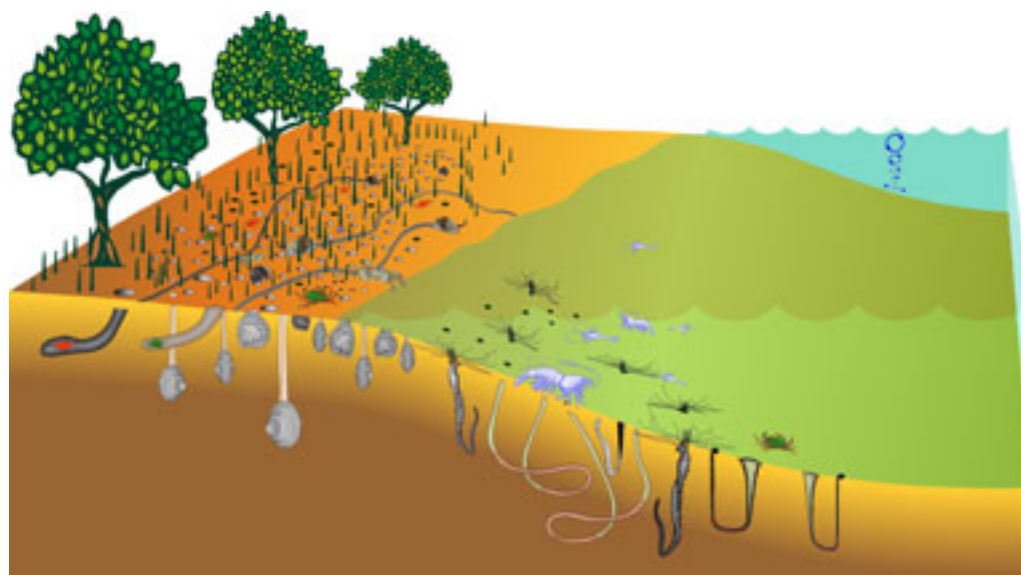


Figure 8.4: Biological and physical processes, such as the burrowing and feeding activities of animals and/or sediment resuspension by waves, mix the upper sediment column. As a result, sediment profiles are modified and limit the temporal resolution of dating. The surface mixed layer (SML) is the yellow zone.

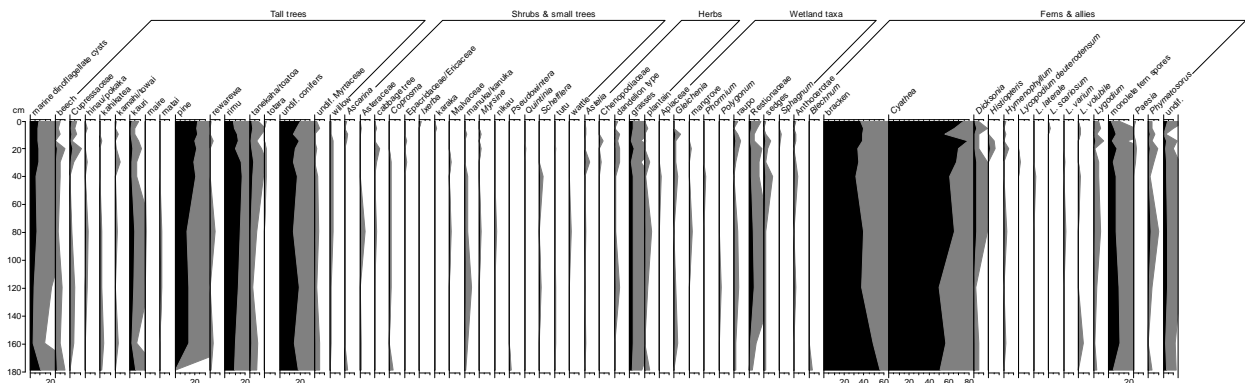


Figure 9.3: Core LC-6 pollen profiles for major plant groups expressed as a percentage of the terrestrial pollen and spore sum.

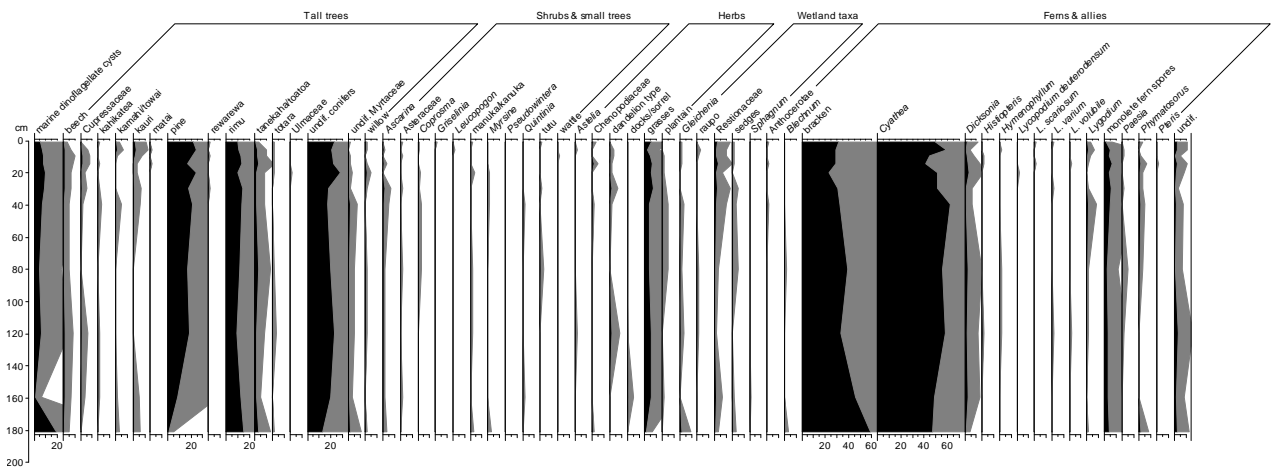


Figure 9.4: Core LC-7 pollen profiles for major plant groups expressed as a percentage of the terrestrial pollen and spore sum.

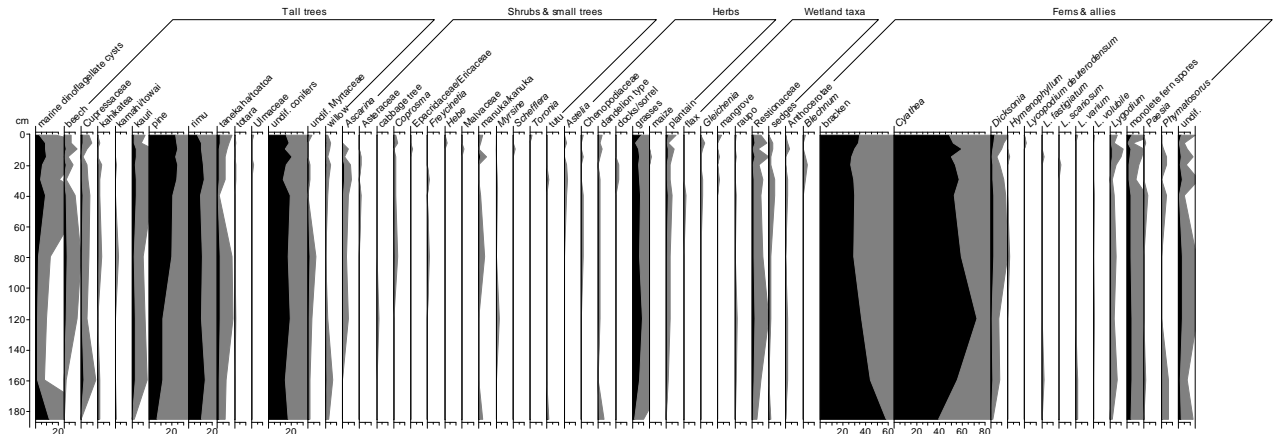


Figure 9.5: Core LC-8 pollen profiles for major plant groups expressed as a percentage of the terrestrial pollen and spore sum.

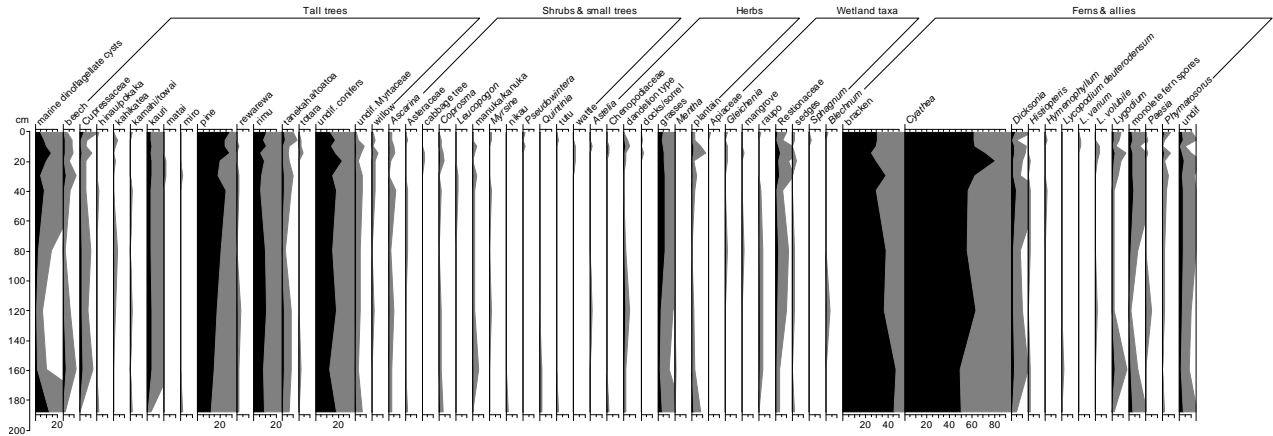


Figure 9.6: Core LC-9 pollen profiles for major plant groups expressed as a percentage of the terrestrial pollen and spore sum.

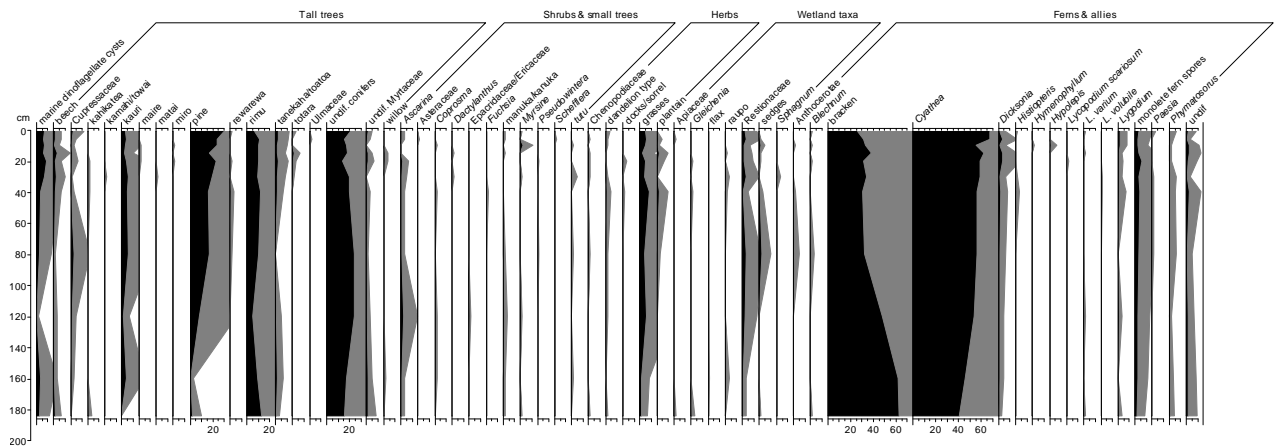


Figure 9.7: Core LC-10 pollen profiles for major plant groups expressed as a percentage of the terrestrial pollen and spore sum.

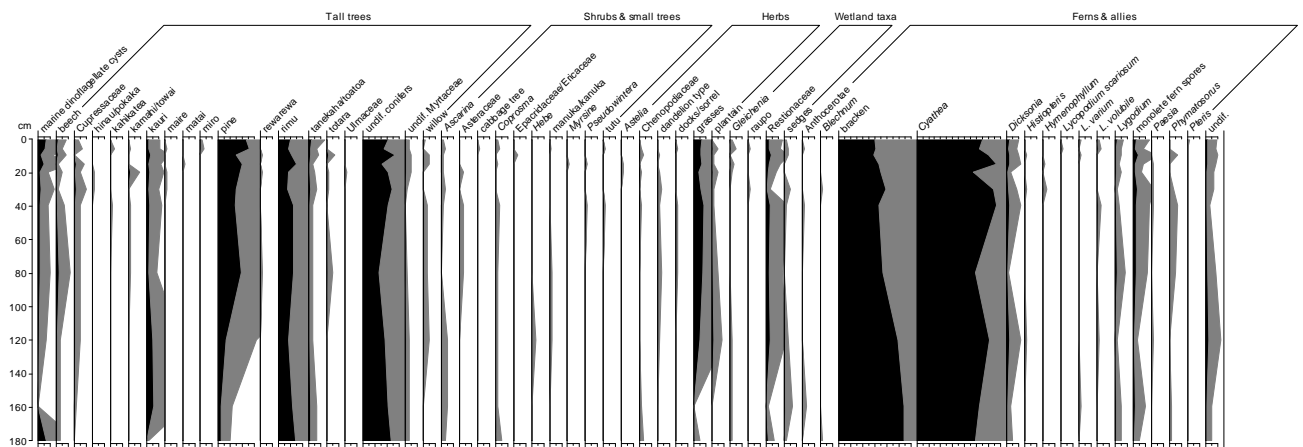


Figure 9.8: Core LC-11 pollen profiles for major plant groups expressed as a percentage of the terrestrial pollen and spore sum.